

# Colloquium: Strongly interacting photons in one-dimensional continuum

Dibyendu Roy

Max Planck Institute for the Physics of Complex Systems,  
Nöthnitzer Strasse 38, 01187 Dresden, Germany  
and Raman Research Institute, Bangalore 560080, India\*

C. M. Wilson

Electrical & Computer Engineering Department and the Institute for Quantum Computing,  
University of Waterloo, Ontario N2L 3G1, Canada

Ofer Firstenberg

Department of Physics of Complex Systems,  
Weizmann Institute of Science, Rehovot 76100, Israel

(published 10 May 2017)

Photon-photon scattering in vacuum is extremely weak. However, strong effective interactions between single photons can be realized by employing strong light-matter coupling. These interactions are a fundamental building block for quantum optics, bringing many-body physics to the photonic world and providing important resources for quantum photonic devices and for optical metrology. This Colloquium reviews the physics of strongly interacting photons in one-dimensional systems with no optical confinement along the propagation direction. It focuses on two recently demonstrated experimental realizations: superconducting qubits coupled to open transmission lines and interacting Rydberg atoms in a cold gas. Advancements in the theoretical understanding of these systems are presented in complementary formalisms and compared to experimental results. The experimental achievements are summarized alongside a description of the quantum optical effects and quantum devices emerging from them.

DOI: [10.1103/RevModPhys.89.021001](https://doi.org/10.1103/RevModPhys.89.021001)

## CONTENTS

I. Introduction	1
II. Single Emitter	3
A. Scattering theory	4
B. Input-output formalism	8
C. Other theoretical techniques	10
D. Three-level emitter: A single-photon router	10
E. Superconducting circuits	12
III. Multiple Emitters in the Strong-coupling Regime	14
A. Photon-mediated interaction between distant emitters	15
B. Small ensemble of adjacent emitters	15
C. Directional photon propagation	15
IV. Multiple Interacting Emitters in the Weak-coupling Regime: Rydberg Polaritons	16
A. Two-photon dynamics	16
B. Many photons	18
C. Limitations and prospects	18
V. Conclusions and Perspectives	18
Acknowledgments	19
Appendix: Derivation of the Input-output Formalism	20
References	20

## I. INTRODUCTION

Photons, the carriers of the electromagnetic force, are elementary particles with no charge and zero rest mass. Photon-photon scattering in vacuum is extremely weak (Karplus and Neuman, 1951; Schwinger, 1951; Iacopini and Zavattini, 1979) and has, in fact, never been experimentally observed at optical or lower frequencies (Zavattini *et al.*, 2012). This makes photons excellent long-distance carriers of classical and quantum information. However, this seclusion of photons poses substantial challenges for efficiently employing them for information processing. In classical communication networks, optical signals are often converted to electrical signals, which can then be manipulated using solid-state devices. However, existing conversion methods are inefficient at the few-photon level and are ill suited for quantum information processing. This has motivated scientists in a number of fields, such as *nonlinear quantum optics* and *cavity quantum electrodynamics*, to study effective photon-photon interactions (Gibbs, 1985) with the ultimate goal of strong and controllable coupling between single photons. Interactions at the single-photon level are essential for a wide variety of quantum optical applications. For instance, they form the basis for all-optical quantum gates (Imamoğlu *et al.*, 1997) and enable metrology beyond the standard quantum limit (Napolitano *et al.*, 2011). They are also important from the

\*Present address.

fundamental physics viewpoint, endowing photonic systems with matterlike properties and realizing strong correlations and quantum many-body behavior in light (Chang *et al.*, 2008; Carusotto and Ciuti, 2013).

Cavity quantum electrodynamics (QED) is a paradigmatic discipline (Miller *et al.*, 2005; Walther *et al.*, 2006; Haroche and Raimond, 2013) exhibiting effective photon-photon interactions in the quantum regime (Birbaum *et al.*, 2005; Schuster *et al.*, 2008). In cavity QED, atoms are placed inside a high-finesse electromagnetic resonator, in which the radiation spectrum is discrete. Bouncing between the resonator mirrors, a single photon effectively interacts with the atoms many times, significantly enhancing the atom-photon coupling. This in turn can generate strong correlations between the photons. Cavity QED experiments with free atoms have been carried out with alkali metals in optical cavities (Thompson, Rempe, and Kimble, 1992; Mabuchi and Doherty, 2002; Birbaum *et al.*, 2005; Dayan *et al.*, 2008; Schuster *et al.*, 2008) and with Rydberg atoms in microwave cavities (Nogues *et al.*, 1999; Raimond, Brune, and Haroche, 2001; Guerlin *et al.*, 2007; Deleglise *et al.*, 2008). Cavity QED experiments have also been conducted on a variety of solid-state systems, including quantum dots (QDs) in photonic crystals (Yoshie *et al.*, 2004; Badolato *et al.*, 2005; Englund *et al.*, 2007; Hennessy *et al.*, 2007; Fushman *et al.*, 2008; Carter *et al.*, 2013) and superconducting microwave circuits. In the latter, known as circuit QED (Blais *et al.*, 2004; Chiorescu *et al.*, 2004; Wallraff *et al.*, 2004; Girvin, Devoret, and Schoelkopf, 2009), superconducting qubits acting as artificial atoms are coupled to microwave photons in Fabry-Pérot cavities made of coplanar waveguides as shown in Fig. 1(a). Both the fields of cavity and circuit QED have been very successful, providing both significant fundamental results and important advances in quantum information science. Nevertheless, the cavities used to enhance the coupling in these systems also present several disadvantages, for instance, the narrow bandwidth of the emitted photons and the problem of stochastic release of photons by the cavity (Hoi *et al.*, 2012). A related challenge is the coupling of photons into and out of the cavities with high efficiency, as is required to link large numbers of nodes in quantum networks (Aoki *et al.*, 2009).

Because of these limitations, much recent work has focused on cavity-free systems. The coupling strength in these system can be quantified by the extinction of a propagating photon by a single emitter ( $1 - T$ ), where  $T$  is the transmission coefficient. Although the nomenclature is still settling, a reasonable definition of strong coupling in these open systems is that

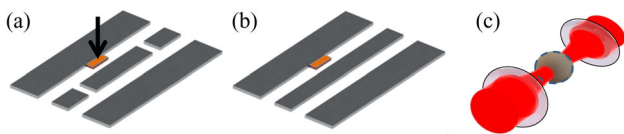


FIG. 1. (a) A superconducting qubit (marked with an arrow) embedded in a one-dimensional transmission line waveguide. A cavity is formed by two capacitive gaps in the middle conductor. (b) Without the cavity. (c) Probe light focused through a dense atomic cloud, exciting a single Rydberg atom within the blockade sphere (dashed line).

$1 - T > 50\%$ , which implies that the emission rate from the atom into the desired mode is larger than the decoherence rate associated with all other processes, including emission into other modes. van Enk and Kimble (2001) and Zumofen *et al.* (2008) showed theoretically that a single atom can fully block ( $1 - T = 100\%$ ) photons in open space, if their spatial and temporal modes match the atomic radiation pattern, while a tightly focused beam is limited to  $1 - T < 85\%$ . In both cases, photons are transversely focused to an area  $A$  comparable with the scattering cross section of the atom  $\sigma_a$ , and their electric field becomes large enough to excite the atom with near unity probability. The highest extinction by a single emitter experimentally achieved in three-dimensional (3D) open space is  $1 - T = 30\%$  (Maser *et al.*, 2016).

A major barrier to higher extinction in open space is the spatial-mode mismatch between the incident and scattered waves. This problem was recently solved in two complementary ways, leading to strong coupling and photon-photon interactions in cavity-free one-dimensional (1D) systems.

(i) *Superconducting qubits in open transmission lines*, which are related to circuit QED systems, as illustrated in Fig. 1(b). These systems enhance the coupling in two ways, both inherited from circuit QED. Most importantly, superconductors can confine the microwave fields to deeply subwavelength sizes in the transverse dimensions. This produces a mode volume, in units of cubic wavelengths, that is orders of magnitude smaller than that of 3D cavities or free fields. In addition, transition dipoles of superconducting qubits are much larger than those of real atoms. These effects together allow for the observation of strong coupling (Astafiev, Zagoskin *et al.*, 2010), extinctions of  $1 - T > 99\%$  (Hoi *et al.*, 2011), and strong photon-photon correlations (Hoi *et al.*, 2012).

(ii) *Rydberg atoms excited by focused optical beams in a dense atomic gas*. In these systems, strong coupling is achieved by greatly enhancing the size of the effective scatterer, thereby achieving mode matching to collimated light beams. The dipolar interaction between Rydberg atoms prevents the excitation of more than one Rydberg atom inside the volume of a so-called *blockade sphere*. With only zero or one excitation, each blockade sphere thus acts as a “superatom” (Vuletic, 2006). The weak coupling of photons to each individual atom can sum up in a dense gas to a strong effective coupling with the superatoms, leading to extinction of  $1 - T \geq 95\%$  (Baur *et al.*, 2014). As long as the blockade sphere is wider than the beam waist, as illustrated in Fig. 1(c), the evolution is limited to the longitudinal 1D continuum. Photon-photon interactions were observed in this system, with photons either blocking (Peyronel *et al.*, 2012) or spatially attracting (Firstenberg *et al.*, 2013) each other.

These cavity-free systems feature intrinsically nonequilibrium, quantum many-body dynamics. The input field is driven by either a laser or microwave generator, imposing a nonequilibrium boundary condition on the propagating photons in 1D. Therefore, the study of photon-photon correlation mediated by local light-matter coupling in 1D calls for advanced quantum field theories in the strongly interacting and nonequilibrium regimes. Traditionally, photon transport in this type of system is studied by employing a master equation that assumes a weak coherent state as input and

usually involves approximations such as linearization of operator equations (see Sec. II.B for details) and the Markovian approximation (Agarwal, 2013). Here we review the recent progress in developing new analytical and numerical techniques to study collective scattering of multiple photons from two-, three-, or multilevel emitters in a 1D continuum.

This Colloquium presents an overview of this research, emphasizing the systems discussed. Other 1D systems with artificial atoms, which are outside the scope of this paper, include QDs coupled to surface plasmons of a metallic nanowire (Akimov *et al.*, 2007; Akselrod *et al.*, 2014; Versteegh *et al.*, 2014) or to line defects in photonic crystals (Laucht *et al.*, 2012; Arcari *et al.*, 2014; Javadi *et al.*, 2015; Lodahl, Mahmoodian, and Stobbe, 2015), and QDs or nanocrystals coupled to semiconductor or diamond nanowires (Babinec *et al.*, 2010; Claudon *et al.*, 2010; Reithmaier *et al.*, 2015). In addition, strong coupling to single emitters in 1D can also be achieved in an ion trap (Meir *et al.*, 2014), with cold atoms trapped inside (Bajcsy *et al.*, 2009) or near (Vetsch *et al.*, 2010) an optical fiber, or with single molecules doped in an organic crystal inside a glass capillary (Faez *et al.*, 2014).

In Sec. II, we summarize the theoretical approaches and experimental results for systems with single emitters, along with a systematic description of various phenomena and their application to quantum information processing. Theories and experiments with multiple emitters are presented in Sec. III in the strong-coupling regime, and in Sec. IV in the weak-coupling regime in systems of interacting Rydberg atoms. We conclude with a short discussion on current research challenges in Sec. V.

## II. SINGLE EMITTER

A model configuration of a two-level emitter (2LE) side coupled to photons in a waveguide is shown in Fig. 2(a). This is a common model for superconducting qubits coupled to a transmission line (Wallraff *et al.*, 2004; Astafiev, Zagoskin *et al.*, 2010; Hoi *et al.*, 2012) and for QDs coupled to surface plasmons (Akimov *et al.*, 2007). The model in Fig. 2(b) has the 2LE directly coupled to the photons in the waveguide. This model is popular for atomic cavity QED experiments (Birbaum *et al.*, 2005) and is also often used in experiments with line-defect photonic crystals (Faraon *et al.*, 2007; Park *et al.*, 2008). The transmission and reflection of photons in the side-coupled configuration can be mapped to those in the directly coupled configuration (Shen and Fan, 2009).

Our model system also connects to a number of problems important in condensed-matter physics, for instance, the general problem of a quantum tunnel in open (dissipative) systems (Caldeira and Leggett, 1983; Costi and Zarand, 1999)

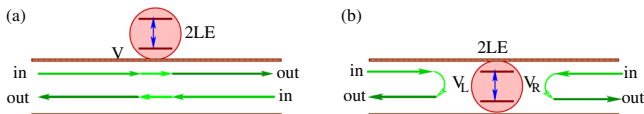


FIG. 2. Two configurations of emitter-photon coupling in an open waveguide: (a) side coupled and (b) direct coupled.

and specifically the spin-boson problem (Leggett *et al.*, 1987), which has seen renewed importance in describing decoherence in various implementations of quantum bits. In the systems of interest in this Colloquium, the photons in the 1D continuum play the role of the bosonic bath in the condensed-matter models. There are also exact analogies to various other nonequilibrium quantum impurity models, including the nonequilibrium Kondo model (Meir, Wingreen, and Lee, 1991; Cronenwett, Oosterkamp, and Kouwenhoven, 1998; Goldhaber-Gordon *et al.*, 1998; Mehta and Andrei, 2006; Dhar, Sen, and Roy, 2008; Nishino, Imamura, and Hatano, 2011). We note, however, that in the condensed-matter context the models are most often concerned with the dynamics of the spin or impurity. In the present work, we are most often concerned with the dynamics of the bath itself, that is, the photons in the 1D continuum. In addition, the bosonic fields considered in most condensed-matter models are actually collective excitations of matter, such as phonons. In that sense, experiments related to these models are not generally concerned with light-matter coupling.

A general Hamiltonian of a 2LE side coupled to photons in a 1D continuum is given by  $\tilde{H} = \tilde{H}_0 + \tilde{H}_1$ , where

$$\tilde{H}_0 = \int dk \hbar \omega_k a_k^\dagger a_k + \hbar(\tilde{\omega}_e - i\gamma)|e\rangle\langle e|, \quad (1)$$

$$\tilde{H}_1 = \int dk \hbar V_k (a_k^\dagger |g\rangle\langle e| + |e\rangle\langle g| a_k). \quad (2)$$

The first term in Eq. (1) represents the propagating photon fields of frequency  $\omega_k$  and wave vector  $k$ . The 2LE is described by the second term in Eq. (1), with transition frequency  $\tilde{\omega}_e$  between states  $|g\rangle$  and  $|e\rangle$ . The  $i\gamma$  term accounts for spontaneous emission into photon modes outside of the 1D continuum, which dominates in atomic systems (Shen and Fan, 2009). In Secs. II.B and II.E, we discuss how to treat pure dephasing, which dominates in superconducting systems. The interaction of the propagating photons with the 2LE is governed by  $\tilde{H}_1$ , which is written in the rotating-wave approximation. This is valid for typical light-matter coupling strengths available in recent experiments. Here  $a_k$  ( $a_k^\dagger$ ) is the photon annihilation (creation) operator, and the coupling strength of a photon of wave vector  $k$  with the emitter is  $V_k$ .

The energy-momentum dispersion ( $\omega_k$  vs  $k$ ) of photons in various 1D waveguides is generally nonlinear and depends on the properties of the waveguide. However, it is convenient to assume linear dispersion to describe the first two theoretical approaches discussed here. We can linearize the dispersion near some arbitrary frequency  $\omega_0$  with the corresponding wave vector  $\pm k_0$  as shown in Fig. 3. The approximate linearized dispersion of  $\omega_k$  around  $k_0$  (right-moving photons) and  $-k_0$  (left-moving photons) reads

$$\begin{aligned} \int_{k=k_0} \omega_k a_k^\dagger a_k &\approx \int_{k=k_0} [\omega_0 + v_g(k - k_0)] a_{R,k}^\dagger a_{R,k}, \\ \int_{k=-k_0} \omega_k a_k^\dagger a_k &\approx \int_{k=-k_0} [\omega_0 - v_g(k + k_0)] a_{L,k}^\dagger a_{L,k}, \end{aligned} \quad (3)$$

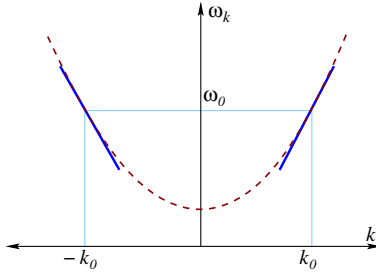


FIG. 3. Linearization of the dispersion relation of the waveguide mode. The full dispersion relation  $\omega_k$  is shown by the dashed curve. The linearized relations are denoted by the two solid lines around the wave vectors  $\pm k_0$ , corresponding to a frequency  $\omega_0$ .

where  $a_{R,k}^\dagger$  ( $a_{L,k}^\dagger$ ) creates a right- (left-) moving photon and  $v_g$  is the group velocity of photons at  $\omega_0$ . Thus we divide the propagating photons into two oppositely moving modes (channels). Next we extend the limits of the integration over  $k$  to  $(-\infty, \infty)$  for the left- and right-moving photons, as we are interested only in photons with a narrow bandwidth in the vicinity of  $\omega_0$ , and we make a change of variables  $k \mp k_0 \rightarrow k$  for the right- and left-moving photons.

The total excitation operator  $N_E = \int dk [a_{R,k}^\dagger a_{R,k} + a_{L,k}^\dagger a_{L,k}] + |e\rangle\langle e|$  commutes with the linearized Hamiltonian  $\tilde{H}$ . Subtracting the term  $\hbar\omega_0 N_E$  from the linearized  $\tilde{H}$  gives the final Hamiltonian  $H = \tilde{H} - \hbar\omega_0 N_E = H_0 + H_1$ , where

$$\begin{aligned} \frac{H_0}{\hbar} &= \int_{-\infty}^{\infty} dk v_g k (a_{R,k}^\dagger a_{R,k} - a_{L,k}^\dagger a_{L,k}) \\ &\quad + (\omega_e - i\gamma) |e\rangle\langle e|, \\ \frac{H_1}{\hbar} &= \int_{-\infty}^{\infty} dk [V_k (a_{R,k}^\dagger + a_{L,k}^\dagger) |g\rangle\langle e| + \text{H.c.}], \end{aligned} \quad (4)$$

with  $\omega_e = \tilde{\omega}_e - \omega_0$ .

Several interrelated theoretical techniques have been employed in recent years for investigating correlated photon dynamics in a 1D continuum. We can divide them into five different groups: (a) multiparticle scattering theory in a continuum (Shen and Fan, 2007a, 2007b; Yudson and Reineker, 2008; Roy, 2010a; Zheng, Gauthier, and Baranger, 2010), (b) the input-output formalism of quantum optics (Fan, Kocabaş, and Shen, 2010; Koshino and Nakamura, 2012; Peropadre *et al.*, 2013), (c) an approach based on the Lippmann-Schwinger equation (Roy, 2011a; Zheng and Baranger, 2013), (d) a method based on the Lehmann-Symanzik-Zimmermann reduction for the multiphoton scattering process (Shi and Sun, 2009), and (e) the time-dependent, wave-packet evolution approach (Longo, Schmitteckert, and Busch, 2010). Scattering theory is a well-known framework to study scattering of waves and particles within the Schrödinger picture of quantum mechanics, and it has been extensively applied in different branches of physics. The input-output formalism was mainly developed for understanding light-matter interaction, and it is based on the Heisenberg picture. In what follows, we carefully discuss these two techniques and the connection between them. We

briefly mention the applications of the other approaches later on.

### A. Scattering theory

In scattering theory, the scattering matrix  $S$  expresses how an incoming state of monochromatic, free photons evolves via a local interaction with atoms into a superposition of outgoing monochromatic photons. The  $S$  matrix for scattering of an  $N$ -photon state is defined by (Newton, 1982; Taylor, 2006)

$$S_{\mathbf{p};\mathbf{k}}^{(N)} = \langle \mathbf{p} | S | \mathbf{k} \rangle, \quad (5)$$

where  $|\mathbf{k}\rangle$  and  $|\mathbf{p}\rangle$  are incoming and outgoing photonic states, respectively. Here the vectors  $\mathbf{k}$  and  $\mathbf{p}$  denote the incoming and outgoing momenta of the  $N$  photons. These incoming and outgoing states are considered to be free states in the interaction picture, and they exist long before ( $t_0 \rightarrow -\infty$ ) and long after ( $t_1 \rightarrow \infty$ ) the scattering occurs. The operator

$$S = \lim_{\substack{t_0 \rightarrow -\infty \\ t_1 \rightarrow \infty}} U_I(t_1, t_0)$$

is given by the time-evolution operator  $U_I$  in the interaction picture  $U_I(t_1, t_0) = e^{iH_0 t_1/\hbar} e^{-iH(t_1-t_0)/\hbar} e^{-iH_0 t_0/\hbar}$ , and the  $S$  matrix can be redefined as

$$\langle \mathbf{p} | S | \mathbf{k} \rangle = \langle \mathbf{p}^- | \mathbf{k}^+ \rangle. \quad (6)$$

The scattering eigenstates  $|\mathbf{k}^+\rangle$  and  $|\mathbf{p}^-\rangle$  evolve in the interaction picture from a free-photon state in either the distant past or the distant future:

$$\begin{aligned} |\mathbf{k}^+\rangle &= U_I(0, t_0) |\mathbf{k}\rangle = e^{iH t_0/\hbar} e^{-iH_0 t_0/\hbar} |\mathbf{k}\rangle = \Omega_+ |\mathbf{k}\rangle, \\ |\mathbf{p}^-\rangle &= U_I(0, t_1) |\mathbf{p}\rangle = e^{iH t_1/\hbar} e^{-iH_0 t_1/\hbar} |\mathbf{p}\rangle = \Omega_- |\mathbf{p}\rangle, \end{aligned}$$

where we drop the limits of  $t_0, t_1$  for compactness and imply  $t_0 \rightarrow -\infty$  and  $t_1 \rightarrow \infty$  in all forthcoming similar expressions. It is also possible to introduce input and output operators  $a_{i_m, \text{in}}^\dagger(k_m)$  and  $a_{o_m, \text{out}}^\dagger(p_m)$ , respectively, which create the incoming and outgoing scattering eigenstates such that

$$\begin{aligned} S_{\mathbf{p};\mathbf{k}}^{(N)} &= \langle \mathbf{p} | S | \mathbf{k} \rangle = \langle \mathbf{p}^- | \mathbf{k}^+ \rangle \\ &= \langle \varphi | a_{o_1, \text{out}}(p_1) \cdots a_{o_N, \text{out}}(p_N) a_{i_1, \text{in}}^\dagger(k_1) \cdots a_{i_N, \text{in}}^\dagger(k_N) | \varphi \rangle, \end{aligned} \quad (7)$$

where  $|\varphi\rangle$  is the vacuum state, and

$$a_{i_m, \text{in}}(k_m) = \Omega_+ a_{i_m, k_m} \Omega_+^\dagger, \quad (8)$$

$$a_{o_m, \text{out}}(k_m) = \Omega_- a_{o_m, k_m} \Omega_-^\dagger, \quad (9)$$

with the commutation relations

$$\begin{aligned} [a_{i_m, \text{in}}(k_m), a_{i_n, \text{in}}^\dagger(k_n)] &= \delta(k_m - k_n) \delta_{i_m, i_n}, \\ [a_{o_m, \text{out}}(p_m), a_{o_n, \text{out}}^\dagger(p_n)] &= \delta(p_m - p_n) \delta_{o_m, o_n}. \end{aligned}$$

The indices  $i_m, o_m$  can take on the values  $L, R$  for  $m = 1, 2, \dots, N$ , depending on whether the  $m$ th incoming or outgoing photon is left moving or right moving. The connection of these input and output operators to those in the input-output formalism will become clear in the next section.

Shen and Fan (2007a, 2007b) recently developed a method inspired by the nonperturbative Bethe-ansatz calculation to derive exact scattering eigenstates  $|\mathbf{k}^+\rangle$  of a few photons. The incoming and outgoing photon states can be obtained from the scattering eigenstate  $|\mathbf{k}^+\rangle$ . The dynamics of two photons in this system are very different from those of a single photon, as they become correlated via the collective scattering from the 2LE (Rupasov and Yudson, 1984a, 1984b; Deutsch, Chiao, and Garrison, 1992; Cheng and Kurizki, 1995). The approach we present treats the atom-photon dynamics in real space, which is particularly convenient for discussing steady-state photon transport from one space-time point to another.

We start with an ansatz for the full scattering eigenstate  $|\mathbf{k}^+\rangle$  of  $H$  for a particular unscattered state  $|\mathbf{k}\rangle$  of  $H_0$ . The total number of photons  $N$  is conserved during the scattering process when using the rotating-wave approximation. To calculate different amplitudes of the scattering eigenstate, we employ the time-independent Schrödinger equation  $H|\mathbf{k}^+\rangle = \hbar v_g(k_1 + k_2 + \dots + k_N)|\mathbf{k}^+\rangle$  with boundary conditions that determine the propagation direction of the incident photons. We now write down an effective representation of  $H$  in real space, where the evolution of the incident photons is more conveniently described. To this end, we take the photon operators in momentum space to be the Fourier transforms of real-space operators, for example,

$$a_{R,k} = \frac{1}{\sqrt{2\pi}} \int_{-\infty}^{\infty} dx a_R(x) e^{-ikx},$$

where  $a_R(x)$  annihilates a right-moving photon at position  $x$  (Shen and Fan, 2009). Thus, we find an effective real-space Hamiltonian for a 2LE coupled to 1D continuum with linear dispersion,

$$\begin{aligned} \frac{H_{\text{eff}}}{\hbar} = & -i \int dx v_g \left[ a_R^\dagger(x) \frac{\partial}{\partial x} a_R(x) - a_L^\dagger(x) \frac{\partial}{\partial x} a_L(x) \right] \\ & + (\omega_e - i\gamma) |e\rangle \langle e| + V[(a_R^\dagger(0) + a_L^\dagger(0)) |g\rangle \langle e| + \text{H.c.}] \end{aligned} \quad (10)$$

We assumed here that the coupling  $V_k \equiv V/\sqrt{2\pi}$  is independent of the wave vector  $k$  (the Markov approximation). The Hamiltonian  $H_{\text{eff}}$  is non-Hermitian in the presence of the dissipation term  $\gamma$ . In the following, we calculate  $|\mathbf{k}^+\rangle$  using the Hermitian  $H_{\text{eff}}$  without  $\gamma$ , and subsequently replace  $\omega_e$  by  $\omega_e - i\gamma$  in the final results (Rephaeli and Fan, 2013).

The incident photons can be injected in the right-moving and/or left-moving channels. The nonequilibrium dynamics can be probed in experiments by measuring the transmission and reflection of photons at the opposite sides of the waveguide. For a side-coupled 2LE, the transmission coefficient is calculated from the number of photons remaining in the incident channel (or channels) after scattering, and the reflection coefficient is determined by counting photons in

the opposite channel (or channels) after scattering. For example, the transmission and reflection coefficients for  $N$  right-moving incident photons are, respectively,

$$\begin{aligned} T &= \frac{\langle \mathbf{k}^+ | a_R^\dagger(x) a_R(x) | \mathbf{k}^+ \rangle}{\langle \mathbf{k} | a_R^\dagger(x) a_R(x) | \mathbf{k} \rangle}, \\ R &= \frac{\langle \mathbf{k}^+ | a_L^\dagger(x') a_L(x') | \mathbf{k}^+ \rangle}{\langle \mathbf{k} | a_R^\dagger(x') a_R(x') | \mathbf{k} \rangle}, \end{aligned}$$

where the denominators are a measure of the incident photon flux and are independent of  $x, x'$ . Here we choose  $x > 0$  and  $x' < 0$ . Both  $T$  and  $R$  provide information only about average photon transport in the waveguide. Assessing other statistics of the scattered photons, such as fluctuations in the photon number, requires calculating higher-order correlation functions.

We now calculate the single-photon and two-photon scattering eigenstates for the Hamiltonian  $H_{\text{eff}}$  following Roy (2010a) and Zheng, Gauthier, and Baranger (2010).

*Single-photon dynamics:* The state of an incident photon in the right-moving channel is  $|k\rangle = \int dx e^{ikx} a_R^\dagger(x) |\varphi\rangle / \sqrt{2\pi}$ , where  $|\varphi\rangle$  represents the photon vacuum with the 2LE in the ground state. Considering different scattering processes, we write an ansatz for the scattering eigenstate,

$$|k^+\rangle = \int dx [g_R(x) a_R^\dagger(x) + g_L(x) a_L^\dagger(x) + \delta(x) e_k |e\rangle \langle g|] |\varphi\rangle,$$

where  $g_R(x)$  and  $g_L(x)$  are amplitudes for right-moving and left-moving photons, respectively, and  $e_k$  is the excitation amplitude for the 2LE. Using the Schrödinger equation  $H_{\text{eff}}|k^+\rangle = \hbar v_g k |k^+\rangle$ , we obtain three coupled linear equations for these three unknown amplitudes

$$\begin{aligned} v_g \left( -i \frac{\partial}{\partial x} - k \right) g_R(x) + V e_k \delta(x) &= 0, \\ v_g \left( i \frac{\partial}{\partial x} - k \right) g_L(x) + V e_k \delta(x) &= 0, \\ (\omega_e - i\gamma - v_g k) e_k + V [g_R(0) + g_L(0)] &= 0. \end{aligned} \quad (11)$$

Their solutions with the boundary conditions  $g_R(x < 0) = e^{ikx}/\sqrt{2\pi}$ ,  $g_L(x > 0) = 0$  and the continuity relation  $g_{R/L}(0) = [g_{R/L}(0+) + g_{R/L}(0-)]/2$  are

$$\begin{aligned} g_R(x) &\equiv g_k(x) = \frac{e^{ikx}}{\sqrt{2\pi}} [\theta(-x) + t_k \theta(x)], \\ g_L(x) &= \frac{e^{-ikx}}{\sqrt{2\pi}} r_k \theta(-x), \\ e_k &= \frac{1}{\sqrt{2\pi}} \frac{V}{v_g k - \omega_e + i(\gamma + \Gamma)}, \end{aligned} \quad (12)$$

where  $\theta(x)$  is the step function. Here  $\Gamma = V^2/v_g$ , and we identify  $2\Gamma$  as the energy relaxation rate of the emitter into the output channels. The transmission amplitude  $t_k$  and reflection amplitude  $r_k$  are given by

$$t_k = \frac{v_g k - \omega_e + i\gamma}{v_g k - \omega_e + i(\gamma + \Gamma)}, \quad r_k = t_k - 1, \quad (13)$$

yielding the normalized one-photon reflection and transmission coefficients

$$R(k) = |r_k|^2 = \frac{\Gamma^2}{(v_g k - \omega_e)^2 + (\gamma + \Gamma)^2}, \quad (14)$$

$$T(k) = |t_k|^2 = \frac{(v_g k - \omega_e)^2 + \gamma^2}{(v_g k - \omega_e)^2 + (\gamma + \Gamma)^2}. \quad (15)$$

In the absence of loss ( $\gamma = 0$ ),  $R(k) + T(k) = 1$ , and the one-photon reflection exhibits a Breit-Wigner-like (Lorentzian) line shape around the resonance  $v_g k = \omega_e$ , as shown in Fig. 4. An incident, resonant photon is totally reflected by the emitter. Thus, a lossless side-coupled emitter behaves as a perfect mirror for propagating photons in a 1D continuum (Shen and Fan, 2005a, 2005b).

Several features of these one-photon line shapes, including both the real and imaginary parts of  $t_k$  and  $r_k$ , were observed in the optical regime in various *cavity* QED setups (Birnbau et al., 2005). For example, a 40% reflection of weak coherent light was obtained with microtoroidal cavities interacting with single cesium atoms (Dayan et al., 2008; Aoki et al., 2009), as depicted in Figs. 5(a) and 5(b). The observation of photon antibunching [Fig. 5(d)] in the reflected signal demonstrated that it was dominated by single photons. The coupling to and from the cavity was implemented with a tapered optical fiber in the so-called overcoupled regime and thus dominated the internal system losses (Aoki et al., 2009). The one-photon line shapes were also demonstrated with a photonic crystal nanocavity coupled to a semiconductor QD (Englund et al., 2007; Fushman et al., 2008). In a *1D continuum*, strong scattering of single photons by a single emitter was first observed for microwave photons in superconducting circuits by Astafiev, Zagoskin et al. (2010). Similar scattering line shapes were later observed for microwave and optical photons in various 1D settings (Abdumalikov et al., 2010; Hoi et al., 2011; Goban et al., 2014). This strong scattering of single photons has been exploited to construct various all-optical quantum devices, such as a one-photon quantum switch (Zhou et al., 2008), quantum memory, and quantum gates (Koshino, Ishizaka, and Nakamura, 2010; Ciccarello et al., 2012;

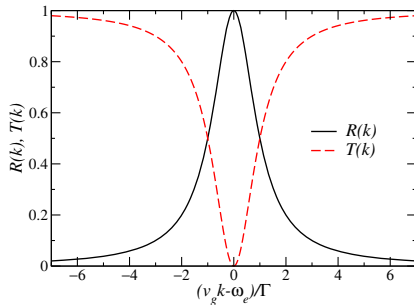


FIG. 4. The reflection coefficient (solid line) and transmission coefficient (dashed line) of a single photon propagating in a 1D continuum with a side-coupled lossless two-level emitter.

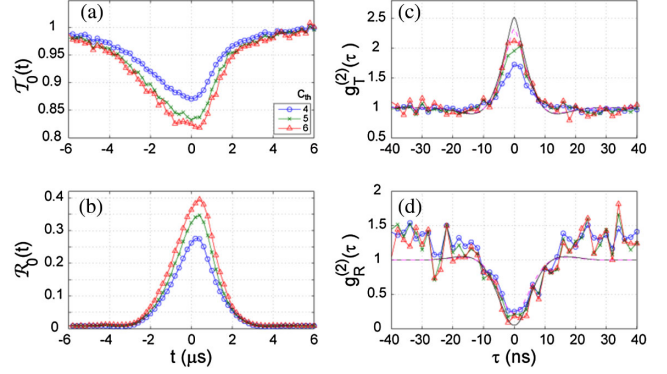


FIG. 5. Reflection of single photons from a coherent-state input by one atom near a microtoroidal cavity. (a) Transmission  $\mathcal{T}_0(t)$  and (b) reflection  $\mathcal{R}_0(t)$  of the probe field after averaging over atom transit events with a selection criterion that the sum of the counts over a time interval of  $4 \mu\text{s}$  is equal to or greater than a threshold count  $C_{\text{th}}$  shown in the legend of (a). (c), (d) The second-order (intensity) correlation functions  $g_{T,R}^{(2)}(\tau)$  for the transmitted and reflected fields. The dip in  $g_R^{(2)}(\tau)$  around  $\tau = 0$  indicates anticorrelation in the detection of photons, which is a signature of antibunching and indicates that the field is dominated by single photons. Solid lines are a theoretical calculation described in Aoki et al. (2009). Adapted from Aoki et al., 2009.

Zheng, Gauthier, and Baranger, 2013; Rosenblum, Borne, and Dayan, 2015).

*Two-photon dynamics:* The dynamics of two photons strongly coupled to a single emitter in 1D is interesting and nontrivial. A 2LE is saturated by a single resonant photon, and a second photon in the waveguide cannot be absorbed by the excited emitter. Rephaeli and Fan (2012) showed that the outcome of the interaction depends on the spectral bandwidth of the second photon's wave packet. If the extent of the wave packet is much longer than the spontaneous emission lifetime  $(\Gamma + \gamma)^{-1}$  of the emitter, the excited emitter first decays to the ground state and then completely reflects the second photon. In the opposite limit of an extremely short wave packet, the emitter-photon interaction is inhibited, and the second photon is fully transmitted. In both limits, the first and second photons interact independently with the emitter and thus remain uncorrelated. However, for the intermediate regime, the second photon stimulates the relaxation of the emitter to the ground state. The two photons then leave the emitter simultaneously, becoming correlated. This stimulated emission in a 1D continuum is special, as the emission enhancement cannot be entirely attributed to photon indistinguishability, but largely results from the photon correlation generated by the emitter (Rephaeli and Fan, 2012).

We construct a two-photon scattering eigenstate in 1D that covers all of the limits. First we write the incident state for two photons with wave vectors  $\mathbf{k} = (k_1, k_2)$  in the right-moving channels

$$|\mathbf{k}\rangle = \int dx_1 dx_2 \phi_{\mathbf{k}}(x_1, x_2) \frac{1}{\sqrt{2}} a_R^\dagger(x_1) a_R^\dagger(x_2) |\varphi\rangle, \quad (16)$$

where  $\phi_{\mathbf{k}}(x_1, x_2) = (e^{ik_1x_1+ik_2x_2} + e^{ik_1x_2+ik_2x_1})/(2\sqrt{2\pi})$ . Our ansatz for the two-photon scattering eigenstate is

$$\begin{aligned} |\mathbf{k}^+\rangle = & \int dx_1 dx_2 \left[ g_{RR}(x_1, x_2) \frac{1}{\sqrt{2}} a_R^\dagger(x_1) a_R^\dagger(x_2) \right. \\ & + e_R(x_1) \delta(x_2) a_R^\dagger(x_1) |e\rangle \langle g| \\ & + g_{RL}(x_1; x_2) a_R^\dagger(x_1) a_L^\dagger(x_2) \\ & + e_L(x_2) \delta(x_1) a_L^\dagger(x_2) |e\rangle \langle g| \\ & \left. + g_{LL}(x_1, x_2) \frac{1}{\sqrt{2}} a_L^\dagger(x_1) a_L^\dagger(x_2) \right] |\varphi\rangle, \end{aligned} \quad (17)$$

where  $g_{RR}(x_1, x_2)$ ,  $g_{RL}(x_1, x_2)$ , and  $g_{LL}(x_1, x_2)$  are two-photon amplitudes, and  $e_R(x_1)$  and  $e_L(x_2)$  are amplitudes of right- and left-moving photons with the 2LE in the excited state. These five unknown amplitudes can be found by solving five coupled linear differential equations, obtained from the two-photon stationary Schrödinger equation  $H_{\text{eff}}|\mathbf{k}^+\rangle = \hbar v_g(k_1 + k_2)|\mathbf{k}^+\rangle$ . One can solve the differential equations with boundary conditions  $g_{RR}(x_1, x_2 < 0) = \phi_{\mathbf{k}}(x_1, x_2)$ ,  $g_{LL}(x_1, x_2 > 0) = 0$ , and  $g_{RL}(x_1 < 0; x_2 > 0) = 0$  for the unscattered state in Eq. (16), and continuity relations for the amplitudes, e.g.,  $g_{RR}(0, x) = g_{RR}(x, 0) = [g_{RR}(0+, x) + g_{RR}(0-, x)]/2$ . For example, the amplitudes of the right-moving photons in terms of  $g_{\mathbf{k}}(x)$  and  $e_{\mathbf{k}}$  in Eqs. (12) are

$$\begin{aligned} g_{RR}(x_1, x_2) = & \frac{1}{\sqrt{2}} \left[ g_{k_1}(x_1) g_{k_2}(x_2) + 2 \frac{\Gamma}{v_g} e_{k_1} e_{k_2} e^{i(k_1+k_2)x_c} \right. \\ & \left. \times e^{i(k_1+k_2-2\omega_e/v_g)x/2} e^{-(\gamma+\Gamma)x/v_g} \theta(x) \theta(x_2) \right] \\ & + (x_1 \leftrightarrow x_2), \end{aligned} \quad (18)$$

$$\begin{aligned} e_R(x_1) = & [g_{k_1}(x_1) e_{k_2} + g_{k_2}(x_1) e_{k_1}] \\ & + 2i \frac{V}{v_g} e_{k_1} e_{k_2} e^{i(v_g k_1 + v_g k_2 - \omega_e + i\gamma + i\Gamma)x_1/v_g} \theta(x_1), \end{aligned} \quad (19)$$

where  $x_c = (x_1 + x_2)/2$  and  $x = x_1 - x_2$ . We observe that the second terms in  $g_{RR}(x_1, x_2)$  and  $e_R(x_1)$  decay to zero with increasing  $|x_1 - x_2|$  and  $|x_1|$ , respectively. These terms are regarded as *two-photon bound states*.

Recently, the existence of two-particle bound states in the presence of a localized interaction was discussed in the contexts of both photon (Shen and Fan, 2007b; Liao and Law, 2010) and electron transport (Dhar, Sen, and Roy, 2008; Nishino, Imamura, and Hatano, 2011). Because the interaction is spatially confined, energy and momentum can be exchanged and redistributed between the photons (with the constraint of fixed total energy), enabling the development of photon-photon correlations. The correlation strength depends on  $\Gamma$ . Experimental evidence for the two-photon bound state appears in second-order correlation measurements and the transmission and reflection coefficients of the scattered fields (Hoi *et al.*, 2012; Firstenberg *et al.*, 2013), which we discuss later.

It is interesting to study the asymptotic behavior (away from the emitter) of the two-photon scattering eigenstate

$$\begin{aligned} |\mathbf{k}^{a+}\rangle = & \int dx_1 dx_2 [rt(x_1, x_2) a_R^\dagger(x_1) a_L^\dagger(x_2) \\ & + \frac{r_2(x_1, x_2)}{\sqrt{2}} a_L^\dagger(x_1) a_L^\dagger(x_2) \\ & + \frac{t_2(x_1, x_2)}{\sqrt{2}} a_R^\dagger(x_1) a_R^\dagger(x_2)] |\varphi\rangle, \end{aligned}$$

where  $t_2(x_1, x_2)$ ,  $r_2(x_1, x_2)$ , and  $rt(x_1, x_2)$  are two-photon amplitudes where, respectively, both photons are transmitted, both are reflected, and one is transmitted and the other reflected. When two degenerate incident photons are resonant with the lossless emitter ( $v_g k_1 = v_g k_2 = \omega_e$  and  $\gamma = 0$ ), we find (Shen and Fan, 2007a)

$$t_2(x_1, x_2) = -\frac{1}{\sqrt{2\pi}} e^{2i\omega_e x_c/v_g} e^{-\Gamma|x|/v_g}, \quad (20)$$

$$r_2(x_1, x_2) = \frac{1}{\sqrt{2\pi}} e^{-2i\omega_e x_c/v_g} (1 - e^{-\Gamma|x|/v_g}), \quad (21)$$

$$rt(x_1, x_2) = -\frac{1}{\pi} e^{i\omega_e x/v_g} e^{-2\Gamma|x_c|/v_g}. \quad (22)$$

Two important following points to notice from these expressions are (1) the outgoing state is not a product state, and (2) the transmitted photons are *bunched*, whereas the reflected photons are *antibunched*. Here the separation  $x$  between the two scattered photons is equivalent to a time delay between them. When plotted versus  $x$  in Fig. 6,  $|t_2(x_1, x_2)|^2$  shows a cusp, and  $|r_2(x_1, x_2)|^2$  shows a dip at  $x = 0$ . For a side-coupled 2LE, since  $r_2(x_1, x_2)$  arises entirely from emission without any contribution from the incident photons, the antibunching in  $r_2(x_1, x_2)$  confirms that a single emitter cannot simultaneously emit two photons. On the other hand, the behavior of  $t_2(x_1, x_2)$  and  $rt(x_1, x_2)$  involves interference between the incident and emitted photons. The behaviors of  $r_2(x_1, x_2)$  and  $t_2(x_1, x_2)$  in Fig. 6 agree qualitatively with the experimentally measured two-photon correlations  $g^{(2)}(\tau)$  of reflected and transmitted photons, shown in Figs. 5(c) and 5(d) and 12 for optical and microwave photons.

An exact multiphoton scattering state for 2LEs (Zheng, Gauthier, and Baranger, 2010) and multilevel emitters (Zheng, Gauthier, and Baranger, 2012; Roy and Bondyopadhyaya,

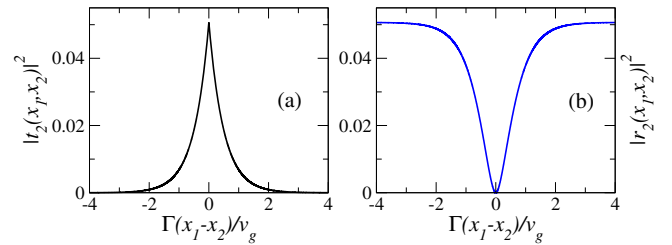


FIG. 6. Correlations between scattered photons in the lossless resonant case. The calculated two-photon scattering coefficients  $|t_2|^2$  and  $|r_2|^2$  are plotted vs the scaled separation  $\Gamma(x_1 - x_2)/v_g$ . (a) Bunching of transmitted photons indicated by the peak in  $|t_2|^2$  at  $x_1 = x_2$ . (b) Antibunching of reflected photons indicated by  $|r_2|^2 = 0$  at  $x_1 = x_2$ .

2014) has been derived, extending the scattering theory. Multiphoton bound states appear in these multiphoton scattering states. The “brute force” technique we used for constructing the scattering eigenstates becomes much more laborious with increasing photon number  $N$ , as the possible scattering configurations rapidly increase. An efficient method to describe the evolution of an arbitrary initial state of the present system was developed by [Yudson and Reineker \(2008\)](#) using the algebraic Bethe ansatz. This elegant method avoids both the difficulty of following numerous configurations and the subtle problems of normalization and completeness of states. However, with increasing photon number it becomes very difficult to extract useful information from these exact multiphoton scattering states, whether calculated using the algebraic Bethe ansatz or scattering theory.

**Coherent-state input:** Coherent states are an important class of multiphoton states, describing the output of both an ideal laser and a microwave generator. They are thus commonly used as an input in experiments. [Zheng, Gauthier, and Baranger \(2010\)](#) formulated the scattering of a weak coherent-state wave packet by a 2LE using the  $S$  matrix in scattering theory. The incident wave packet is  $|\alpha\rangle = e^{a^\dagger - \bar{n}/2}|\varphi\rangle$ , where  $\bar{n} = \int dk |\alpha(k)|^2$  is the mean photon number, which is kept small  $\bar{n} \leq 1$  to observe few-photon behavior. For a coherent-state wave packet, the photon statistics are Poissonian, implying that the variance of the photon number is also  $\bar{n}$ . Here  $a^\dagger_\alpha = \int dk \alpha(k) a^\dagger_{R,k}$  for an incident wave packet from the left. We employ a Gaussian wave packet ([Zheng, Gauthier, and Baranger, 2010](#))

$$\alpha(k) = \frac{\sqrt{\bar{n}}}{(2\pi\Delta_k^2)^{1/4}} \exp\left(-\frac{(k-k_0)^2}{4\Delta_k^2}\right),$$

with width  $\Delta_k$  and mean momentum  $k_0$ . The scattered state can be expressed as  $|\psi_\alpha^{\text{out}}\rangle = \sum_N S^{(N)}|\alpha\rangle$ , where  $S^{(N)}$  is the  $S$ -matrix operator of  $N$  incident photons, whose elements can be calculated using scattering theory. For example,  $S^{(0)} = |\varphi\rangle\langle\varphi|$  and

$$S^{(1)} = \int dk t_k a^\dagger_{R,k} |\varphi\rangle\langle\varphi| a_{R,k} + \int dk r_k a^\dagger_{L,k} |\varphi\rangle\langle\varphi| a_{R,k},$$

where  $t_k$  and  $r_k$  are the one-photon transmission and reflection amplitudes of Eq. (13). Following this prescription, we find the transmission of a weak coherent-state input

$$\begin{aligned} T(k_0, \Delta_k) &= \frac{\langle\psi_\alpha^{\text{out}}| a^\dagger_R(x) a_R(x) |\psi_\alpha^{\text{out}}\rangle}{\langle\alpha| a^\dagger_R(x) a_R(x) |\alpha\rangle} \\ &= \frac{\int dk_1 dk_2 \alpha(k_1) \alpha(k_2) t_{k_1} t_{k_2}^* e^{i(k_1-k_2)x}}{\int dk_1 dk_2 \alpha(k_1) \alpha(k_2) e^{i(k_1-k_2)x}}, \end{aligned} \quad (23)$$

where  $x > 0$ , and we have kept only the leading order contribution coming from single-photon scattering. For a long, monochromatic pulse ( $\Delta_k \ll \Gamma + \gamma$ ), the coefficient  $T(k_0, \Delta_k)$  reduces to the single-photon transmission coefficient  $T(k_0)$  in Eq. (15).

In experiments, the statistics of scattered photons is predominately determined by measuring second-order

correlations of the scattered fields. For the transmitted beam, it is defined as

$$g^{(2)}(x_1, x_2) = \frac{\langle\psi_\alpha^{\text{out}}| a^\dagger_R(x_1) a^\dagger_R(x_2) a_R(x_2) a_R(x_1) |\psi_\alpha^{\text{out}}\rangle}{\prod_{i=1}^2 \langle\psi_\alpha^{\text{out}}| a^\dagger_R(x_i) a_R(x_i) |\psi_\alpha^{\text{out}}\rangle}.$$

By neglecting the contributions from  $N \geq 3$  photons in  $|\psi_\alpha^{\text{out}}\rangle$  for  $\bar{n} \leq 1$ , [Zheng, Gauthier, and Baranger \(2010\)](#) found

$$\begin{aligned} g^{(2)}(x_2 - x_1) &= \frac{|\int dk_1 dk_2 \alpha(k_1) \alpha(k_2) (t_{k_1} t_{k_2} - r_{k_1} r_{k_2} e^{-(\Gamma+\gamma)|x|/v_g})|^2}{|\int dk_1 dk_2 \alpha(k_1) \alpha(k_2) t_{k_1} t_{k_2}|^2}. \end{aligned} \quad (24)$$

Here again the distance separation can be converted to time separation via  $\tau = (x_2 - x_1)/v_g$ , which is what is typically measured in experiments. The first and second terms in the numerator of Eq. (24) are related, respectively, to the non-interacting and the bound-state parts of the two-photon wave function. Without the bound-state contribution (i.e., no effective photon-photon interaction),  $g^{(2)}(x_2 - x_1) = 1$ . In the presence of the bound state,  $g^{(2)}(x_2 - x_1)$  can show bunching and antibunching of the transmitted photons at different values of the coupling rate  $\Gamma$ , as shown in Fig. 7. Note that the observability of these effects also depends on having the appropriate value of  $\Gamma/\gamma$ . For very strong coupling  $\Gamma/\gamma \gg 1$ ,  $g^{(2)}(x_2 - x_1)$  of the transmitted photons always shows bunching [Fig. 7(c)] and was observed by [Hoi \*et al.\* \(2012\)](#). For very weak coupling  $\Gamma/\gamma \ll 1$ ,  $g^{(2)}(x_2 - x_1)$  is nearly featureless, exhibiting only a small antibunching dip [Fig. 7(a)]. In the intermediate regime  $\Gamma/\gamma \approx 1$ , the antibunching is more pronounced [Fig. 7(b)].

## B. Input-output formalism

The input-output formalism is a celebrated technique for analyzing the effect of light-matter interactions on the quantum statistics of light fields ([Gardiner and Collett, 1985](#); [Walls and Milburn, 2008](#)). Based on the Heisenberg picture, it allows one to study the time evolution of the field operators, with the ability to account for various input field states, for

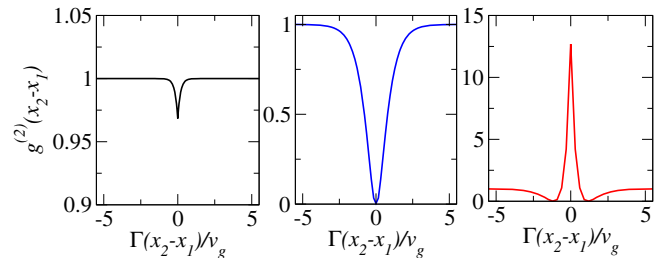


FIG. 7. Second-order correlation function of the transmitted field at various emitter-photon coupling strengths for a coherent-state input with  $\bar{n} \leq 1$ . The couplings are (left)  $\Gamma/\gamma = 0.2$ , (middle)  $\Gamma/\gamma = 1.6$ , and (right)  $\Gamma/\gamma = 3$ . Here  $v_g k_0 = \omega_e = 10\gamma$  and  $\Delta_k/\gamma = 1$ . Note the different vertical scales. The second-order correlation shows antibunching and bunching at different coupling strengths.

example, coherent states, Fock states, or squeezed states. Fan, Kocabaş, and Shen (2010) recently adopted this formalism to investigate the few-photon scattering by emitters in a 1D continuum, relating it to the scattering theory of correlated photons.

*Equations of motion:* Essentially, given a Hamiltonian  $H$ , one uses the Heisenberg picture to derive a set of nonlinear differential equations for the time evolution of the input and output fields  $b_{m,\text{in}}(t)$ ,  $b_{m,\text{out}}(t)$  of left-moving ( $m = L/+$ ) and right-moving ( $m = R/-$ ) photons,

$$b_{m,\text{in}}(t) = \frac{1}{\sqrt{2\pi}} \int dk a_{m,k}(t_0) e^{imv_g k(t-t_0)}, \quad (25)$$

$$b_{m,\text{out}}(t) = \frac{1}{\sqrt{2\pi}} \int dk a_{m,k}(t_1) e^{imv_g k(t-t_1)}, \quad (26)$$

where  $a_{m,k}(t_0) = e^{iHt_0/\hbar} a_{m,k} e^{-iHt_0/\hbar}$  and  $a_{m,k}(t_1) = e^{iHt_1/\hbar} a_{m,k} e^{-iHt_1/\hbar}$  are Heisenberg operators in the limits  $t_0 \rightarrow -\infty$ ,  $t_1 \rightarrow \infty$ . For clarity, we use  $b$ ,  $b^\dagger$  for operators in the input-output formalism and  $a$ ,  $a^\dagger$  for operators in scattering theory. The input-output operators are directly related to the operators that create and destroy incoming and outgoing scattering eigenstates in scattering theory [see Eqs. (8) and (9)]. For example,

$$\begin{aligned} b_{R,\text{in}}(t) &= \frac{1}{\sqrt{2\pi}} \int dk e^{iHt_0/\hbar} a_{R,k} e^{-iHt_0/\hbar} e^{-iv_g k(t-t_0)} \\ &= \frac{1}{\sqrt{2\pi}} \int dk e^{iHt_0/\hbar} e^{-iH_0 t_0/\hbar} a_{R,k} e^{iH_0 t_0/\hbar} e^{-iHt_0/\hbar} e^{-iv_g k t} \\ &= \frac{1}{\sqrt{2\pi}} \int dk a_{R,\text{in}}(k) e^{-iv_g k t}, \end{aligned} \quad (27)$$

where in the second line we replaced  $a_{R,k} e^{iv_g k t_0}$  with  $e^{-iH_0 t_0/\hbar} a_{R,k} e^{iH_0 t_0/\hbar}$  by employing  $[H_0, a_{R,k}] = -\hbar v_g k a_{R,k}$ . Thus,  $a_{m,\text{in/out}}(k)$  gives the spectral representation of  $b_{m,\text{in/out}}(t)$ . Using relations similar to Eq. (27), we can rewrite the  $S$ -matrix elements in Eq. (7) as

$$\begin{aligned} S_{\mathbf{p},\mathbf{k}}^{(N)} &= \langle \mathbf{p} | S | \mathbf{k} \rangle \\ &= \langle \varphi | a_{o_1,\text{out}}(p_1) \cdots a_{o_N,\text{out}}(p_N) a_{i_1,\text{in}}^\dagger(k_1) \cdots a_{i_N,\text{in}}^\dagger(k_N) | \varphi \rangle \\ &= \mathcal{F}\mathcal{T}^{2N} \langle \varphi | b_{o_1,\text{out}}(t_1) \cdots b_{o_N,\text{out}}(t_N) b_{i_1,\text{in}}^\dagger(t_1') \cdots \\ &\quad \times b_{i_N,\text{in}}^\dagger(t_N') | \varphi \rangle, \end{aligned} \quad (28)$$

where we use a global Fourier transform  $\mathcal{F}\mathcal{T}^{(2N)} = (2\pi)^{-N} \int \prod_{j=1}^N dt_j dt_j' e^{iv_g(i_j k_j t_j' - o_j p_j t_j)}$  with  $i_j, o_j = -(R), +(L)$  to relate the  $S$  matrix in linearized momentum (or frequency) and time. We now show how the  $S$ -matrix elements are found within the input-output formalism.

To simplify the presentation, we slightly rewrite the emitter part in the Hamiltonian  $H$  using Pauli matrices. We write the full Hamiltonian for a single 2LE side coupled to a 1D continuum as

$$\begin{aligned} \frac{H_{io}}{\hbar} &= \int_{-\infty}^{\infty} dk v_g k (a_{R,k}^\dagger a_{R,k} - a_{L,k}^\dagger a_{L,k}) + \frac{1}{2} \omega_e \sigma_z \\ &\quad + \frac{V}{\sqrt{2\pi}} \int_{-\infty}^{\infty} dk [(a_{R,k}^\dagger + a_{L,k}^\dagger) \sigma_- + \sigma_+ (a_{R,k} + a_{L,k})], \end{aligned} \quad (29)$$

where  $\sigma_\pm$  are raising and lowering operators for the 2LE and  $\sigma_z = 2\sigma_+ \sigma_- - 1$ . Here  $\omega_e$  is again the transition energy of the 2LE, and we dropped the inelastic loss term  $i\gamma$ . We again assume that the coupling  $V$  to the linearized modes is independent of the wave vector  $k$ .

One can write Heisenberg equations of motion for the operators in Eq. (29) and define input-output operators for the fields, as illustrated in detail for a chiral model in the Appendix. One then gets

$$\begin{aligned} b_{R,\text{out}}(t) &= b_{R,\text{in}}(t) - i \frac{V}{v_g} \sigma_-(t), \\ b_{L,\text{out}}(t) &= b_{L,\text{in}}(t) - i \frac{V}{v_g} \sigma_-(t), \\ \frac{d\sigma_-}{dt} &= -(i\omega_e + \Gamma) \sigma_- + iV \sigma_z [b_{R,\text{in}}(t) + b_{L,\text{in}}(t)], \end{aligned} \quad (30)$$

again denoting  $\Gamma = V^2/v_g$ . We now have all the required tools to study the scattering of photons in this system.

*Scattering properties:* The one-photon scattering properties are encoded in the one-photon  $S$  matrix. For a single, right-moving input photon, the transmission amplitude is given by the following element of the  $S$  matrix:

$$\langle \varphi | a_{R,\text{out}}(p) a_{R,\text{in}}^\dagger(k) | \varphi \rangle = \frac{1}{\sqrt{2\pi}} \int dt \langle \varphi | b_{R,\text{out}}(t) | k^+ \rangle e^{iv_g p t}, \quad (31)$$

where we use  $a_{R,\text{in}}^\dagger(k) | \varphi \rangle = | k^+ \rangle$  [see Eq. (7)] and write  $a_{R,\text{out}}(p)$  in terms of  $b_{R,\text{out}}(t)$ . We therefore need to calculate  $\langle \varphi | b_{R,\text{out}}(t) | k^+ \rangle$  to find the one-photon transmission amplitude. It can be obtained by sandwiching Eqs. (30) between  $\langle \varphi |$  and  $| k^+ \rangle$ ,

$$\langle \varphi | b_{R/L,\text{out}}(t) | k^+ \rangle = \langle \varphi | b_{R/L,\text{in}}(t) | k^+ \rangle - i \frac{V}{v_g} \langle \varphi | \sigma_-(t) | k^+ \rangle, \quad (32)$$

$$\begin{aligned} \frac{d}{dt} \langle \varphi | \sigma_- | k^+ \rangle &= -(i\omega_e + \Gamma) \langle \varphi | \sigma_- | k^+ \rangle \\ &\quad + iV \langle \varphi | \sigma_z [b_{R,\text{in}}(t) + b_{L,\text{in}}(t)] | k^+ \rangle. \end{aligned} \quad (33)$$

One can easily find some parts of these expressions,

$$\begin{aligned} \langle \varphi | b_{R,\text{in}}(t) | k^+ \rangle &= \langle \varphi | b_{R,\text{in}}(t) a_{R,\text{in}}^\dagger(k) | \varphi \rangle = \frac{e^{-iv_g k t}}{\sqrt{2\pi}}, \\ \langle \varphi | b_{L,\text{in}}(t) | k^+ \rangle &= \langle \varphi | b_{L,\text{in}}(t) a_{R,\text{in}}^\dagger(k) | \varphi \rangle = 0, \\ \langle \varphi | \sigma_z b_{R,\text{in}}(t) | k^+ \rangle &= -\langle \varphi | b_{R,\text{in}}(t) | k^+ \rangle, \end{aligned} \quad (34)$$

where  $\sigma_z|\varphi\rangle = -|\varphi\rangle$ , as  $|\varphi\rangle$  is the photon vacuum state with the 2LE also in its ground state. Plugging the results of Eqs. (34) into Eq. (33), we obtain a first-order inhomogeneous differential equation with the solution

$$\langle\varphi|\sigma_-|k^+\rangle = \frac{e^{-i v_g k t}}{\sqrt{2\pi}} \frac{V}{v_g k - \omega_e + i\Gamma}, \quad (35)$$

$$\langle\varphi|b_{R,\text{out}}(t)|k^+\rangle = \frac{\tilde{t}_k e^{-i v_g k t}}{\sqrt{2\pi}}. \quad (36)$$

Here  $\tilde{t}_k = t_k(\gamma = 0)$  is the one-photon transmission amplitude ignoring decoherence and photon loss. Finally, inserting Eq. (36) into Eq. (31), we arrive at

$$\langle\varphi|a_{R,\text{out}}(p)a_{R,\text{in}}^\dagger(k)|\varphi\rangle = \tilde{t}_k \delta(k - p). \quad (37)$$

Similarly, we can derive the one-photon reflection amplitude  $\tilde{r}_k = \tilde{t}_k - 1$  from the  $S$ -matrix element  $\langle\varphi|a_{L,\text{out}}(p)a_{R,\text{in}}^\dagger(k)|\varphi\rangle = \tilde{r}_k \delta(k + p)$ . We thus see that the one-photon scattering amplitudes obtained here are the same as those we found using scattering theory.

We note that the same result can also be arrived at by directly approximating  $\sigma_z = -1$  in Eqs. (30), thus linearizing the operator equations. Such an approximation is commonly used in many quantum optics calculations in the weak-excitation limit by considering the 2LE to be mostly in its ground state. Physically, the weak-excitation limit is valid for one-photon scattering when the one-photon wave packet has a much longer duration than the lifetime of the 2LE. However, the weak-excitation limit is not always valid, even for a one-photon pulse (Rephaeli, Shen, and Fan, 2010).

Similar derivations of the elements of the  $S$  matrix are carried out for multiphoton Fock states (Fan, Kocabaş, and Shen, 2010; Rephaeli, Kocabaş, and Fan, 2011; Xu, Rephaeli, and Fan, 2013) as well as for coherent-state inputs (Koshino and Nakamura, 2012; Peropadre *et al.*, 2013). Input-output theory can also be easily extended using the master equation formalism to include decoherence processes such as pure dephasing, which dominates in superconducting systems (Koshino and Nakamura, 2012; Peropadre *et al.*, 2013). Finally, the input-output formalism was recently extended to investigate scattering of multiple photons by multiple interacting and noninteracting emitters in a 1D continuum (Caneva *et al.*, 2015; Xu and Fan, 2015). We discuss these in the next section.

### C. Other theoretical techniques

Until now we have discussed scattering of photons in a 1D continuum with a linearized dispersion relation and the Markov approximation. However, there are examples where the linearization is a poor approximation, and the nonlinearity gives rise to important physical behavior (Zhou *et al.*, 2008; Longo, Schmitteckert, and Busch, 2010; Roy, 2011a). One such case is of coupled resonator arrays, exhibiting a tight-binding dispersion relation that is strongly nonlinear. These structures were realized in photonic crystals (Notomi,

Kuramochi, and Tanabe, 2008) and proposed in superconducting systems (Zhou *et al.*, 2008).

For a sinusoidal tight-binding dispersion, the Hamiltonian in Eqs. (1) and (2) can be rewritten as

$$\begin{aligned} \frac{H_{\text{TB}}}{\hbar} = & -J \sum_{x=-\infty}^{\infty} (a_x^\dagger a_{x+1} + a_{x+1}^\dagger a_x) + (\omega_e - i\gamma) b^\dagger b \\ & + V_0 (a_0^\dagger b + b^\dagger a_0) + \frac{U}{2} b^\dagger b (b^\dagger b - 1), \end{aligned} \quad (38)$$

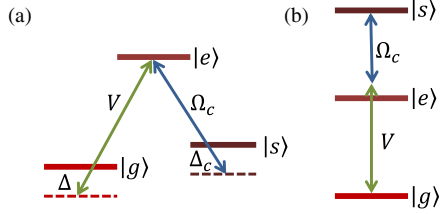
where  $a_x^\dagger$  creates a photon at site  $x$ , and  $J$  is the hopping rate between nearest neighbor sites. Here the 2LE is replaced by an additional bosonic site, side coupled at  $x = 0$  (Longo, Schmitteckert, and Busch, 2010; Roy, 2011a). The photon creation operator at the additional site is  $b^\dagger$ . The states of 0 and 1 photons correspond, respectively, to the ground and the excited states of the 2LE in Eq. (1), whereas the forbidden ‘‘multiphoton’’ occupancy of the 2LE is avoided by introducing the interaction term  $U b^\dagger b (b^\dagger b - 1)/2$  and taking the limit  $U \rightarrow \infty$ .

Scattering eigenstates for one and two photons can be derived exactly for the Hamiltonian in Eq. (38) using the Lippmann-Schwinger equation. Roy (2011a) compared one-photon and two-photon transmission for linear and (nonlinear) tight-binding dispersion relations and pointed out the effect of band edges on the two-photon transmission. Here again the two-photon scattering eigenstates exhibit bound states due to inelastic exchange of photons. A unique feature of this approach is the ability to exactly calculate two-photon scattering states for *multiple* emitters separated by arbitrary distances (Zheng and Baranger, 2013), similarly to the calculation of multiple quantum impurities (Roy, 2010b). Furthermore, one can numerically study two-photon scattering by *multilevel* emitters.

Longo, Schmitteckert, and Busch (2010) investigated the scattering of few-photon states in 1D lattice models using numerical time-dependent wave-packet evolution. This framework allows one to analyze both the dynamics of multiphoton wave packets that interact with the emitter and the dynamics of the emitter itself. Employing the approach of the density matrix renormalization group (DMRG), they extended their study for three-photon and four-photon transport. They demonstrated that a single-particle photon-atom bound state with an energy outside the band can be excited via multiparticle scattering processes, which leads to radiation trapping at the emitter. Another study worth noting is based on the Lehmann-Symanzik-Zimmermann reduction, a method to calculate  $S$ -matrix elements from the time-ordered correlation functions. This approach was employed by Shi and Sun (2009) to investigate multiphoton  $S$  matrices in various complex quantum networks of propagating photons coupled to emitters.

### D. Three-level emitter: A single-photon router

A single-photon router can route one photon from an input port to either of two output ports, while conserving the superposition of input photonic states. It thus finds important applications in optical quantum networks. Building on the


 FIG. 8. (a)  $\Lambda$ -type and (b) ladder-type three-level emitters.

work of [Abdumalikov \*et al.\* \(2010\)](#), [Hoi \*et al.\* \(2011\)](#) demonstrated that a driven three-level emitter (3LE) strongly coupled to a 1D continuum can act as an efficient single-photon router ([Chang \*et al.\*, 2007](#); [Neumeier, Leib, and Hartmann, 2013](#); [Shomroni \*et al.\*, 2014](#)). As we shall see, the presence or absence of a classical control field in this system determines a specific output port for the probe photon.

We consider a 3LE with either the  $\Lambda$  or ladder-type structures in Fig. 8, with the probe light tuned to the  $|g\rangle - |e\rangle$  transition. A classical light field drives the  $|e\rangle - |s\rangle$  transition with a Rabi frequency  $\Omega_c$  and frequency detuning  $\Delta_c$ . The Hamiltonian describing the system

$$\frac{H_R}{\hbar} = \frac{H_{\text{eff}}}{\hbar} + (\omega_e + \Delta_c - i\gamma_s)|s\rangle\langle s| + \frac{\Omega_c}{2}(|s\rangle\langle e| + |e\rangle\langle s|), \quad (39)$$

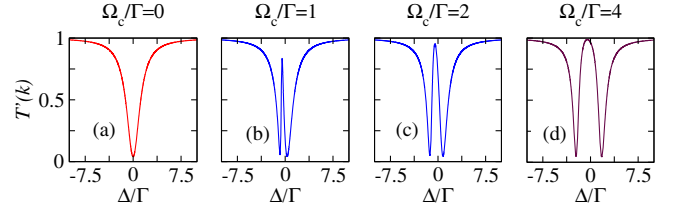
extends the Hamiltonian  $H_{\text{eff}}$  of the 2LE in Eq. (10). Losses from the state  $|s\rangle$  are accounted for by the imaginary term  $-i\gamma_s$ . With natural atoms,  $|g\rangle$  and  $|s\rangle$  can be two different Zeeman states, and the transitions  $|g\rangle - |e\rangle$  and  $|e\rangle - |s\rangle$  couple to different optical polarizations based on selection rules.

[Withaut and Sørensen \(2010\)](#) and [Roy \(2011b\)](#) studied the transmission and reflection line shapes for the  $\Lambda$ -type system. The one-photon transmission and reflection amplitudes are given, respectively, by  $t'_k = \chi/(\chi + i\Gamma)$  and  $r'_k = -i\Gamma/(\chi + i\Gamma)$  [see, e.g., [Roy and Bondyopadhyaya \(2014\)](#) for a derivation], where again  $\Gamma = V^2/v_g$  and

$$\chi = \Delta + i\gamma - \frac{\Omega_c^2}{4(\delta + i\gamma_s)}. \quad (40)$$

Here  $\Delta = v_g k - \omega_e$  is the detuning of the incident probe photon from the  $|g\rangle - |e\rangle$  transition, and  $\delta = \Delta - \Delta_c$  is the Raman detuning. We plot in Fig. 9 the transmission coefficient  $T'(k) = |t'_k|^2$  for different values of the parameters. In the absence of the control field, the probe photon is reflected due to the  $|g\rangle - |e\rangle$  transition [Fig. 9(a)], whereas in the presence of a control, when  $\Omega_c^2 \gtrsim \Gamma\gamma_s$ , a transmission window appears at the Raman resonance  $\Delta = \Delta_c$  ( $\delta = 0$ ) [Figs. 9(b)–9(d)].

Two parameter regimes are of interest. In the first regime, predominantly characterizing atomic  $\Lambda$  systems, the  $|s\rangle$  state is metastable and much longer lived than the  $|e\rangle$  state, that is  $\gamma_s \ll \gamma, \Gamma$ . This yields a narrow transmission window within the broader reflection or absorption line, an effect known as electromagnetically induced transparency (EIT) ([Harris, Field, and Imamoglu, 1990](#); [Boller, Imamoglu, and Harris, 1991](#); [Fleischhauer, Imamoglu, and Marangos, 2005](#)). Intuitively,


 FIG. 9. (a) Perfect reflection, (b), (c) electromagnetically induced transparency at the Raman resonance  $\Delta = \Delta_c$  for weak control field, and (d) Autler-Townes splitting for stronger control fields. The splitting between the Autler-Townes doublet is  $\Omega_c$ . The parameters are  $\Delta_c/\Gamma = -1/2$ ,  $\gamma/\Gamma = 1/4$ , and  $\gamma_s/\Gamma = 1/40$ .

EIT results from a destructive interference between two allowed transitions, leading to cancellation of the population of  $|e\rangle$  and to the formation of a “dark state.” With increasing strength of the control field, the width of the transparency window increases, as shown in Fig. 9(c).

In the second regime, generally characterizing superconducting ladder systems,  $|s\rangle$  is shorter lived than  $|e\rangle$  due to population relaxation, as the  $|s\rangle - |e\rangle$  transition also couples strongly to the transmission line. Therefore  $\gamma_s \gtrsim \gamma, \Gamma$ , and narrow EIT lines cannot be obtained. Rather, stronger control fields  $\Omega_c \gg \Gamma$  are needed to drive the  $|s\rangle - |e\rangle$  transition and open a transparency window ([Anisimov, Dowling, and Sanders, 2011](#)), an effect known as the Autler-Townes splitting (ATS). The width of the transmission window due to ATS is  $\Omega_c$ , as shown in Fig. 9(d). In both regimes, a sufficiently strong control field allows the probe photons to pass the emitter without being reflected. Thus, the presence or absence of a control field determines the route of the probe photon.

The recent experiments by [Abdumalikov \*et al.\* \(2010\)](#) and [Hoi \*et al.\* \(2011\)](#) used a ladder-type superconducting qubit and observed transparency windows due to ATS, as shown in Figs. 10(a) and 10(b). By tuning the control field, [Hoi \*et al.\* \(2011\)](#) demonstrated the routing of a single-photon probe. Since both relaxation and dephasing are important in superconducting systems, a generalized model was introduced by [Abdumalikov \*et al.\* \(2010\)](#) to describe the experiments, replacing the effective non-Hermitian Hamiltonian (39) with a Markovian master equation for the density matrix. The transmission spectra calculated by [Abdumalikov \*et al.\* \(2010\)](#) are shown in Figs. 10(c) and 10(d) and are similar to our  $t'_k$  (with their loss terms  $\gamma_{21}$  and  $\gamma_{31}$  corresponding roughly to our  $\gamma + \Gamma$  and  $\gamma_s$ , respectively).

Recently, more complicated superconducting systems have been used to make effective  $\Lambda$  systems. [Inomata \*et al.\* \(2014\)](#) realized an effective “impedance-matched”  $\Lambda$ -type emitter using dressed states of a driven superconducting qubit-resonator system. [Novikov \*et al.\* \(2016\)](#) demonstrated EIT in a superconducting circuit using the Jaynes-Cummings dressed states of a strongly coupled qubit-cavity system as an effective  $\Lambda$  system.

Photon-photon correlations have also been calculated for 3LE systems ([Li, Huang, and Law, 2015](#)). To do this, one needs to derive the multiphoton scattering states for the system. [Roy \(2011b\)](#) derived the two-photon scattering state of the probe field for a 3LE weakly driven by a control field. An exact two-photon scattering state for an arbitrary strength

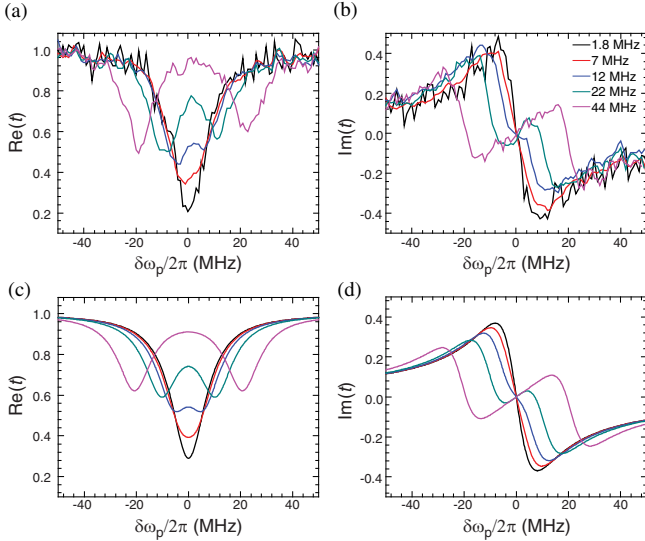


FIG. 10. One-photon transmission amplitudes  $t$  vs the probe detuning  $\delta\omega_p \equiv \Delta$  for a superconducting three-level qubit coupled to a microwave waveguide. (a), (b) The experimentally measured real and imaginary parts of the transmission amplitudes for various control field amplitudes  $\Omega_c$ , specified in (b). The curves show typical dispersion for the Autler-Townes splitting.  $\text{Re}(t)$  near  $\delta\omega_p = 0$  approaches unity with increasing  $\Omega_c$ . (c), (d) Corresponding theoretical curves. Adapted from [Abdumalikov et al., 2010](#).

of  $\Omega_c$  was calculated by [Zheng, Gauthier, and Baranger \(2012\)](#) and [Roy and Bondyopadhaya \(2014\)](#). [Roy and Bondyopadhaya \(2014\)](#) showed that the second-order correlation of the transmitted photons near the Raman resonance changes from bunching to antibunching to constant, as the strength of the control field is ramped up from zero to a higher value where the ATS appears.

### E. Superconducting circuits

While proposed in a variety of experimental systems, the strong coupling of propagating light to matter was first demonstrated in a circuit QED setting, with superconducting qubits playing the role of artificial atoms ([Astafiev, Zagoskin et al., 2010](#)). The major advantage of these types of systems in achieving strong coupling is that the electromagnetic fields can be tightly confined into quasi-1D superconducting waveguides ( $v_g \sim c/3$ ). In a typical implementation, the lateral dimensions are of the order of  $10 \mu\text{m}$  while the corresponding wavelength is of the order of  $10 \text{ mm}$ . (In the direction of propagation, the light is unconfined.) The mode volume is then  $\sim 10^{-6}\lambda^3$ , compared to  $\sim \lambda^3$  for optical systems, implying strongly enhanced electric field strengths. It is, furthermore, straightforward to fabricate superconducting qubits with dipole moments in this range ([Wallraff et al., 2004](#)), meaning that efficient mode matching can be easily accomplished. These were the key insights leading to the rapid growth of experimental work in this field.

These systems work in the microwave regime. In this frequency range ( $\sim 5 \text{ GHz}$ ), where the photon energy  $\hbar\omega$  is well below the superconducting gap energy  $\Delta_{\text{SC}}$ ,

superconductors have very little loss, which protects the coherence of the circuits. In aluminum for instance,  $\Delta_{\text{SC}}/\hbar \approx 50 \text{ GHz}$ . At optical frequencies ( $\hbar\omega \gg \Delta_{\text{SC}}$ ), metals are not superconductors and are very lossy. Therefore, metallic waveguides are not useful in confining optical light at these size scales. The trade-off is that these microwave systems must be operated at very low temperatures, typically below  $50 \text{ mK}$ , in order for the background thermal (blackbody) field to be sufficiently suppressed.

The first demonstration of the strong scattering of propagating microwave light by a single artificial atom was achieved by [Astafiev, Zagoskin et al. \(2010\)](#) from the NEC Corporation group (see Fig. 11). They observed a strong extinction of the transmitted light corresponding to  $1 - T = 94\%$ . This was the first time that the hallmark result of  $1 - T > 50\%$  was achieved for a single scatterer in any type of system, clearly separating the coherent and incoherent scattering regimes. They also derived reflection ( $r$ ) and transmission ( $t$ ) amplitudes of an incident coherent state using input-output theory and the master equation approach to treat decoherence:

$$r = r_0 \frac{1 + i\Delta/\Gamma_2}{1 + (\Delta/\Gamma_2)^2 + \Omega^2/\Gamma_1\Gamma_2}, \quad t = 1 - r, \quad (41)$$

with  $r_0$  the maximal reflection amplitude and  $\Omega$  the Rabi frequency of the incident probe. The rate  $\Gamma_2 = \Gamma_1/2 + \Gamma_\varphi$ , where  $\Gamma_1$  is the energy relaxation rate and  $\Gamma_\varphi$  is the pure dephasing rate. Note that there is a sign difference in the definition of reflection amplitude in Eq. (12) and [Astafiev, Zagoskin et al. \(2010\)](#). For superconducting systems, the rate of emission into spurious modes is negligible, implying  $\Gamma_1 = 2\Gamma$ . For weak driving ( $\Omega \ll \Gamma_1, \Gamma_2$ ), Eq. (41) agrees with Eq. (13) if we further identify  $\Gamma_\varphi = \gamma$ . We note again that this is a typical distinction between atomic and superconducting systems, that is, in the superconducting systems we

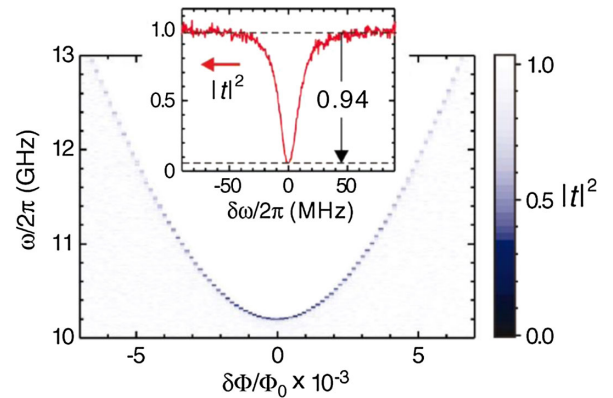


FIG. 11. Spectroscopy of an artificial atom coupled to an open 1D transmission line. The color map shows the power transmission  $T = |t|^2$  vs flux bias  $\delta\Phi$  and incident microwave frequency  $\omega$ . When the incident radiation is on resonance with the emitter, a dip in  $T$  reveals a dark line. Inset:  $|t|^2$  at  $\delta\Phi = 0$  as a function of the probe detuning  $\delta\omega \equiv \Delta$  from the resonance frequency  $\omega_e/2\pi = 10.204 \text{ GHz}$ . The maximal power extinction of  $1 - T = 94\%$  takes place on resonance ( $\delta\omega = 0$ ). Adapted from [Astafiev, Zagoskin et al., 2010](#).

consider here emission into spurious modes is negligible while pure dephasing is significant.

The NEC group demonstrated a number of prototypical atomic physics effects using their artificial atom including resonance fluorescence of the Mollow triplet (Astafiev, Zagoskin *et al.*, 2010; Astafiev, Abdumalikov *et al.*, 2010) and induced transparency due to the Autler-Townes splitting (Abdumalikov *et al.*, 2010) as discussed before. These results demonstrated that the quality of coherence in superconducting qubits had become sufficiently high for them to genuinely be considered “artificial atoms.” NEC’s work was reproduced by the Chalmers group, who improved the scattering efficiency by more than an order of magnitude by increasing the coupling strength, achieving  $1 - T = 99.4\%$  (Hoi *et al.*, 2011; Hoi, Wilson *et al.*, 2013).

Importantly, the simple measurement of the coherent scattering properties at single-photon probe powers can be fully explained by a classical model of scattering from a harmonic oscillator, i.e., an  $LC$  circuit. Essentially, as long as the probe only weakly excites the atom from the ground state, it does not obtain information about the presence of higher levels and cannot distinguish between a two-level and a multilevel system. To rule out that the observed signal is purely classical, we must look beyond the linear response of the system. The experiments mentioned which involve stronger probes and nonlinear response, such as the resonance fluorescence experiment, are not simply explained by a classical model of the emitter. Still, they tell us very little about the state of the scattered electromagnetic field.

As shown theoretically, the light scattered by a single emitter should be distinctly nonclassical, which can be characterized by higher-order correlation measurements. The Chalmers group measured the second-order correlation function  $g^{(2)}(\tau)$  of the scattered field and showed that it was significantly less than 1 (Hoi *et al.*, 2012). The essential idea is that the emitter can scatter only one photon at a time, so it reflects only the one-photon component of the input coherent state, while transmitting the higher photon number components. The reflected state is then a superposition of only the vacuum and the one-photon state, which exhibits photon antibunching as shown in Fig. 12. The antibunching behavior reveals the quantum nature of the scattered field (Kimble, Dagenais, and Mandel, 1977; Paul, 1982).

These circuits have also been explored in terms of possible applications for quantum communication networks. One broad architecture of a network imagines quantum nodes, which perform basic processing tasks, connected by long-distance channels carrying quantum information (Kimble, 2008). By far, the leading candidates for implementing quantum channels involve optical or telecom photons propagating in fibers or free space. A number of physical systems are being actively investigated for implementing quantum nodes (Sherson *et al.*, 2006; DiCarlo *et al.*, 2009; De Greve *et al.*, 2012; Gao *et al.*, 2012; Ritter *et al.*, 2012) with superconducting circuits in open environment being one of the promising candidates.

Using the architecture described previously, the Chalmers group has already demonstrated a number of prototype elements for quantum nodes. In the first experiment, as

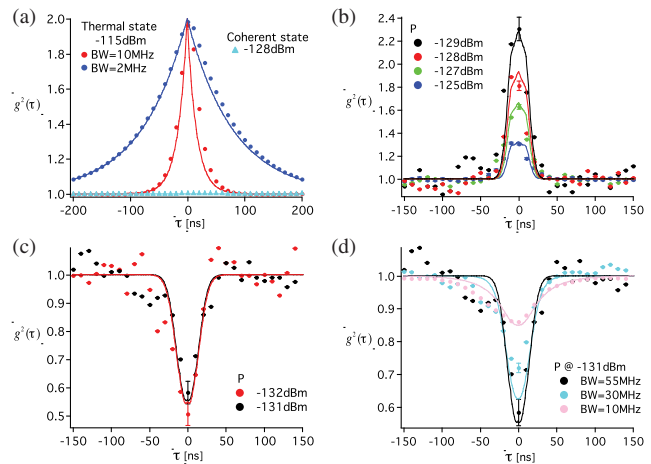


FIG. 12. Second-order correlation function  $g^{(2)}$  vs the time separation  $\tau$  between the photons for a thermal state, a coherent state, and the scattered states generated by the artificial two-level emitter. (a)  $g^{(2)}(\tau)$  of a thermal state and a coherent state. (b)  $g^{(2)}(\tau)$  of the resonant transmitted microwaves for four different incident powers. (c)  $g^{(2)}(\tau)$  of a resonant reflected field for two different incident powers.  $g^{(2)}(0)$  does not reach zero because of well-understood experimental imperfections, including the bandwidth of the measurement system. (d)  $g^{(2)}(\tau)$  of a resonant reflected field for different measurement bandwidths (BW), illustrating how decreasing bandwidth decreases the depth of the dip. The solid curves in (a)–(d) are theory curves. Adapted from Hoi *et al.*, 2012.

mentioned, they demonstrated a router that exploited the ATS to direct a microwave input at the single-photon level between two ports (Hoi *et al.*, 2011). The on-off ratio of the router was 99% with a switching time of a few nanoseconds. The ability to produce nonclassical light, which is a required resource for a quantum network, by scattering classical light from a purely passive device as described earlier (Hoi *et al.*, 2012) also has potential technological applications. This can be considered as a “quantum-state filter” that accepts a desired portion of the input state (the one-photon component) and rejects the rest (the higher photon numbers). We compare this to a conventional frequency filter that accepts a desired set of frequencies while rejecting others. More advanced quantum-state filters, containing multiple qubits, could be an economical way to produce nonclassical light for quantum networks.

In a separate experiment, the Chalmers group demonstrated that the single qubit worked as a highly effective cross-Kerr medium (Hoi, Kockum *et al.*, 2013). The cross-Kerr effect is essentially an effective interaction between light at two different frequencies mediated by a nonlinear medium (Shen, 1984). The basic effect is that the presence of one beam induces a phase shift in the other beam that is proportional to intensity. The cross-Kerr effect was studied extensively in the past as a possible route to quantum nondemolition measurements (QND) of single photons (Munro *et al.*, 2005) and photonic gates (Milburn, 1989; Turchette *et al.*, 1995). However, the strength of the cross-Kerr effect is generally too weak in bulk nonlinear crystal for any of these applications to be realizable. In the Chalmers experiment, by contrast, the bulk nonlinear medium is replaced by a

single three-level (artificial) atom, and the two input fields are tuned to the  $|g\rangle - |e\rangle$  and the  $|e\rangle - |s\rangle$  transition frequencies. The experiment was performed with coherent states, demonstrating an average cross-Kerr phase shift of  $20^\circ$  per photon, surpassing the previous state of the art of  $0.01^\circ$  per photon for propagating light (Matsuda *et al.*, 2009; Perrella *et al.*, 2013; Venkataraman, Saha, and Gaeta, 2013). In parallel, a phase shift of  $45^\circ$  was demonstrated with Rydberg atoms, as discussed in Sec. IV.

This work on the cross-Kerr effect has stimulated a great deal of theoretical work analyzing the prospects of this system to be used for the QND detection of photons. Interestingly, a first work concluded that QND detection could not be achieved with a single atom, due to atomic saturation effects (Fan *et al.*, 2013). Because a bulk nonlinear crystal can largely be considered as an incoherent ensemble of such atoms, this work strongly suggest that QND detection is not possible in a bulk system, which was an important general result. However, subsequent work showed that careful arrangements of multiple atoms, sequentially interacting with the propagating photon, can achieve QND detection of a single propagating photon (Fan *et al.*, 2014; Sathyamoorthy *et al.*, 2014).

The Chalmers group has also looked at a system with one atom in front of a “mirror” (Hoi *et al.*, 2015). In this case, the mirrorlike boundary condition is created by simply terminating the transmission line with a short circuit to ground at one end. The effective separation is modulated around the value of  $\lambda/2$ . Interference between the input field, the field scattered by the atom, and the field reflected by the mirror creates a standing wave pattern. When the separation is exactly  $\lambda/2$ , the atom sits at a node of the field, and it is effectively hidden from the probe. This can be thought of as an interaction between the atom and its image in the mirror, much in the same way that the two real emitters interact in the Zürich experiment (van Loo *et al.*, 2013) described later. Interestingly, it was shown that the atom not only hides from the classical probe field, but also from vacuum fluctuations, with a suppression of the free-space relaxation rate by a factor of 50 being observed. In contrast to the Purcell effect, where a cavity can be used to suppress the relaxation rate, the suppression achieved through this novel form of vacuum engineering occurs even though the atom is coupled to a continuum of propagating states.

While superconducting circuits interacting with microwave photons show great promise for implementing quantum nodes, the implementation of long-distance quantum channels using optical photons is very far advanced, with records distances of  $>100$  for free-space and in-fiber transmissions (Ursin *et al.*, 2007; Korzh *et al.*, 2015). This state of affairs has motivated considerable work in recent years toward the development of a quantum interface between microwave and optical photons. The fundamental difficulty is the several orders of magnitude that separate the energy scales of these two classes of photons. A number of research groups have attempted to bridge this gap in a wide variety of physical systems. One common approach is to use ensembles of dopant atoms in a host crystal, taking advantage of the fact that specific transition can be excited through both microwave and optical Raman transitions. Ensembles are used to enhance the coupling to single photons. A number of different systems are being studied including nitrogen-vacancy centers in diamond

(Amsüss *et al.*, 2011; Kubo *et al.*, 2011; Julsgaard *et al.*, 2013; Grezes *et al.*, 2014; Putz *et al.*, 2014) and rare-earth ions, especially erbium (Bushev *et al.*, 2011; Staudt *et al.*, 2012; Afzelius *et al.*, 2013; Probst *et al.*, 2013). An entirely different approach that has shown promise is to use optomechanical systems, where mechanical vibrations (phonons) in nano-mechanical or micromechanical systems act as an intermediary between the microwave and optical photons (Lin *et al.*, 2010; Bochmann *et al.*, 2013; Andrews *et al.*, 2014). Finally, collective magnon excitations in macroscopic ferrimagnetic crystals are also being studied as a potential medium for an interface (Tabuchi *et al.*, 2014). The shear range of physical systems being studied as a potential implementation of a quantum interface speaks to the compelling nature of the problem.

### III. MULTIPLE EMITTERS IN THE STRONG-COUPLING REGIME

Investigating the interaction of propagating photons with multiple emitters in 1D continuum, as illustrated in Fig. 13, is of fundamental and practical importance. For example, photon-mediated interaction between distant emitters, as recently demonstrated in 1D (Lalumière *et al.*, 2013; van Loo *et al.*, 2013), can be used to generate long-range entanglement between the emitters (Gonzalez-Tudela *et al.*, 2011; Zheng and Baranger, 2013; Greenberg and Shtygashev, 2015). More generally, we can imagine systems with multiple emitters being used in increasingly more advanced quantum communication nodes. Moreover, strong coupling of multiple emitters with propagating photons confined below the diffraction limit has potential practical applications for detection and subwavelength imaging of atoms, ions, molecules, QDs, or color centers in a host crystal (Smolyaninov *et al.*, 2005; Kühn *et al.*, 2006; Chen *et al.*, 2010; Bushev *et al.*, 2011; Rezus *et al.*, 2012; Roy, 2013b). Finally, systems of multiple emitters may realize *photonic* simulators for the quantum many-body dynamics of electrons in condensed matter. Examples of analyzed phenomena in such simulators include a Luttinger liquid of photons (Angelakis *et al.*, 2011), quantum phase transitions of light (Greentree *et al.*, 2006; Hartmann, Brandao, and Plenio, 2006), optical Josephson interferometry (Gerace *et al.*, 2009), and the Tonks-Girardeau gas of photons (Chang *et al.*, 2008).

The potential of multiemitter systems has motivated a number of theoretical studies in recent years. While most have been within the standard Markovian approximation

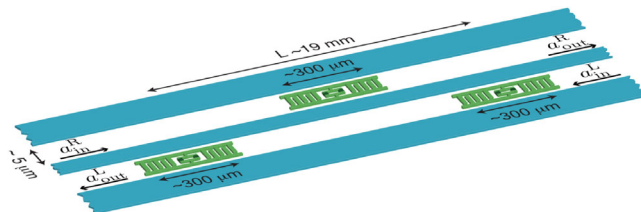


FIG. 13. Photon-mediated interaction between distant emitters in superconducting circuits. Transmon qubits (length  $\approx 300 \mu\text{m}$ ) acting as emitters are coupled to an open 1D transmission line. Adapted from Lalumière *et al.*, 2013.

(Yudson and Reineker, 2008; Dzsojtjan, Sørensen, and Fleischhauer, 2010; Chang *et al.*, 2012; Roy, 2013a; Caneva *et al.*, 2015), others have looked for distinctly non-Markovian effects (Zheng and Baranger, 2013; Laakso and Pletyukhov, 2014).

### A. Photon-mediated interaction between distant emitters

The interaction of an isolated emitter with the vacuum fluctuations of the electromagnetic field leads to the spontaneous emission of real photons and to a renormalization of its transition frequency (Lamb shift) via the emission and absorption of virtual photons. A second emitter in the system can absorb both types of these photons, giving rise to an effective interaction between the two emitters (Goldstein and Meystre, 1997). In a 3D space, the strength of such interaction falls off rapidly with the separation between the emitters because of the large mode volume of the photons and the resulting mode mismatch with the emitters (DeVoe and Brewer, 1996; Eschner *et al.*, 2001). As seen for single emitters, these limitations are mitigated by confining the system to 1D.

Recently, the Zürich group observed clear signatures of photon-mediated interaction between two superconducting transmon qubits (van Loo *et al.*, 2013). The physical separation between the emitters was large enough that there was no direct coupling between them. While the actual separation  $d = 18.6$  mm was fixed in the experiment, the normalized separation  $d/\lambda$ , measured in transition wavelengths, was changed by tuning the transition frequency of the emitter. The normalized separation could be tuned between  $d/\lambda = 1$  and  $d/\lambda = 3/4$ .

For  $d/\lambda = 1$ , the two emitters are driven with the same amplitude and phase by any resonant field in the transmission line. This led to the observation of a superradiant bright state and a subradiant dark state. For  $d/\lambda \sim 3/4$ , one emitter is at a node of the propagating field when the other is at an antinode, suppressing these superradiant effects. However, an exchange interaction mediated by virtual photons is maximized. The anticrossing in the two qubit spectrum caused by this exchange interaction was observed in the resonance fluorescence spectrum of the driven two-emitter system, as shown in Fig. 14. Lalumière *et al.* (2013) described the two-emitter system of the Zürich group using a Markovian master equation along with input-output theory (Lehmberg, 1970), obtaining good agreement with the experimental results.

We note that the coherent exchange mediated by photons can generate a high degree of long-distance entanglement between the emitters (Dzsojtjan, Sørensen, and Fleischhauer, 2010; Gonzalez-Tudela *et al.*, 2011; Fang, Zheng, and Baranger, 2014; Fang and Baranger, 2015; Hensen *et al.*, 2015) which is an important ingredient for quantum information science.

### B. Small ensemble of adjacent emitters

Several studies have been carried out on small ensembles of adjacent emitters with no intrinsic interaction. (We consider intrinsic interactions in Sec. IV.) Rephaeli, Kocabaş, and Fan (2011) calculated two-photon scattering from a pair of

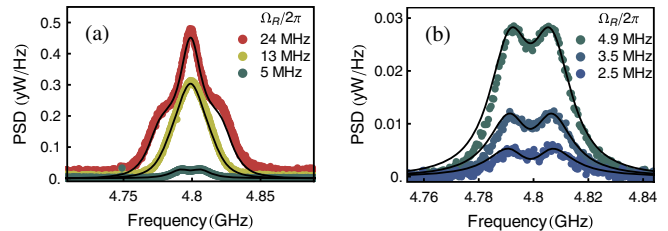


FIG. 14. (a), (b) Photon-mediated exchange interaction between two distant superconducting qubits in an open transmission line. Power spectral density (PSD) of the resonance fluorescence of two qubits in resonance at  $d \sim 3\lambda/4$ , driven at the indicated Rabi rates  $\Omega_R$ . PSD falls with decreasing  $\Omega_R$ . At drive rates much lower than the relaxation rate  $\Omega_R/2\pi \leq 5$  MHz, the observed double-peak structure reveals the effective exchange interaction between the two qubits. Adapted from van Loo *et al.*, 2013.

adjacent 2LEs, predicting that the fluorescence of the emitters is completely quenched for a proper choice of input (Zhou and Swain, 1996). Roy (2013b) compared one-photon and two-photon scattering from two 2LEs versus a single V-type 3LE, showing that the two cases can be distinguished by the statistics of the scattered field. Zapasskii *et al.* (2013) successfully demonstrated this in optical spin-noise spectroscopy experiments.

### C. Directional photon propagation

Strong transverse confinement of guided photons leads to large intensity gradients on the wavelength scale. In this nonparaxial regime, spin (polarization) and orbital angular momentum of light are coupled, an effect known as spin-orbit coupling. In particular, the spin state varies within the transverse plane and along the propagation direction in the waveguide. Interestingly, the local spin of this strongly confined light can be orthogonal to the propagation direction.

Utilizing the spin-orbit coupling, several experimental groups (Petersen, Volz, and Rauschenbeutel, 2014; Le Feber, Rotenberg, and Kuipers, 2015) have recently demonstrated nonreciprocal scattering of light from dipolar scatterers (QDs, gold nanoparticles, alkali atoms) coupled to waveguides (photonic crystals, nanofibers). The propagation direction of scattered light in such systems depends on the spin direction of the incident light. Control of the directionality of the scattering process with over 90% efficiency has been achieved in such nanophotonic waveguide interfaces. Mitsch *et al.* (2014) further showed directional spontaneous emission of photons from emitters into a nanophotonic waveguide. Bliokh, Smirnova, and Nori (2015) argued that the transverse spin in evanescent waves and the spin-controlled directional excitation of surface or waveguide modes is analogous to the quantum spin Hall effect.

Directional propagation due to collective scattering, distinct from these effects, was theoretically studied by Roy (2010a, 2013a) in spatially asymmetric atom-waveguide interfaces. Two different structures were investigated using scattering theory: a 2LE directly coupled to two waveguides with different coupling strengths, and a chain of closely spaced 2LEs with varying transition frequencies (Fratini *et al.*, 2014) along the chain. While the one-photon transmission is

reciprocal in these systems, the two-photon or multiphoton transmission is nonreciprocal due to the broken spatial symmetry. These systems can thus act as optical diodes or isolators (Jalas *et al.*, 2013) for few-photon states.

#### IV. MULTIPLE INTERACTING EMITTERS IN THE WEAK-COUPPLING REGIME: RYDBERG POLARITONS

Up until this point, we explicitly considered only the interaction between photons arising from their coupling to the same emitter. In these configurations, efficient interaction requires the strong-coupling condition  $\Gamma/\gamma \gg 1$ , where the coupling  $\Gamma$  of the emitter to the *confined* probe channel is faster than all other relaxation rates  $\gamma$ , including spontaneous emission to the vacuum environment. In the alternative approach we now discuss, the interaction between photons is obtained without mode confinement in the opposite regime of weak coupling  $\Gamma/\gamma \ll 1$ , by utilizing many atoms, which in turn are intrinsically interacting.

In free space, the cumulative effect of  $N$  atoms is often characterized by the resonant optical depth  $\text{OD} = 2N\Gamma/(\gamma + \Gamma) = N\sigma_a/A$  (Caneva *et al.*, 2015). The atomic cross section  $\sigma_a$  is at most  $\sim\lambda^2$  and typically much smaller than the focused beam area  $A$ , hence high OD are obtained only for large  $N$ . Taking  $t_k$  from Eq. (13), we recover a well-known expression for the total transmission amplitude

$$t_k^N = \exp\left(-\frac{\text{OD}}{2} \frac{i\gamma}{\Delta + i\gamma}\right)$$

at  $\Gamma/\gamma \ll 1$ , where  $\Delta$  is the detuning of the light from resonance. However, contrary to the strong-coupling case, here most of the nontransmitted light is lost rather than reflected. The ratio between the single-atom reflection coefficient  $|r_k|^2$  from Eq. (13) and the loss  $1 - |r_k|^2 - |t_k|^2$  is  $\Gamma/(2\gamma) \ll 1$ . Furthermore, as seen, strong coupling is required for obtaining significant photon-photon correlation (cf. Fig. 7). Indeed while high OD is useful for observing and utilizing single-photon effects, two more ingredients, namely, the cooperative behavior of the atoms and suppression of loss, are required for strong photon-photon interactions in the weak-coupling regime.

Rydberg atoms provide such cooperativity via the dipole blockade mechanism (Lukin *et al.*, 2001). When exciting two or more atoms to Rydberg states—electronic states with a large principal quantum number  $n$  (typically  $n = 40$  to  $100$ )—the dipolar interaction between them shifts their Rydberg levels and consequently their excitation frequency (Reinhard *et al.*, 2007). Below a certain distance between the atoms, known as the blockade radius  $r_B$  (typically  $\leq 10 \mu\text{m}$ ), the frequency shift is larger than the excitation linewidth (typically 1–10 MHz for cold atoms), blocking the excitation of more than one atom. Such large  $r_B$  are achieved at the van der Waals regime, where the frequency shift depends on the extremely large dipoles ( $\sim 10^4$  D) to the power of 4. The blockade effect itself can be used for various quantum information processes with atoms (Müller *et al.*, 2009; Saffman, Walker, and Mølmer, 2010).

The consequence of the dipole blockade for propagating photons is quite intuitively understood. A single photon, exciting a single Rydberg atom, can block the excitation of all  $N_B \gg 1$  atoms in the surrounding virtual sphere of radius  $r_B$ . If the optical depth of the blockade sphere  $\text{OD}_B = N_B\sigma_a/A$  is large, it allows a single photon to significantly alter the optical response for other photons.

The final ingredient required for effective photon-photon interactions in the weak-coupling limit is the suppression of loss, which can be accomplished using EIT as proposed by Friedler *et al.* (2005). A ladder-type configuration as in Fig. 8(b) is used, with a *probe* photon exciting the ground-state atom to an intermediate state, which is coupled to the Rydberg state by a strong *control* field with Rabi frequency  $\Omega_c$ . The probe is transmitted due to EIT within a narrow spectral window. By shifting this window, the dipole blockade disables the EIT for more than one probe photon in the blockade sphere. A strong dependence on the rate of incoming probe photons can be observed by monitoring the average transmission (Pritchard, Weatherill, and Adams, 2013). The optical nonlinear behavior and the emergence of nonclassical correlations during propagation were theoretically investigated within the mean-field approximation by Pritchard *et al.* (2010), Petrosyan, Otterbach, and Fleischhauer (2011), Sevinçli *et al.* (2011), and others.

The transmitted probe experiences strong dispersion and thus reduced group velocity  $v_{\text{EIT}} \ll c$ , where  $c$  is the speed of light in vacuum. It is therefore instructive to view each propagating photon as a slow light-matter polariton (Fleischhauer and Lukin, 2000). Typically these polaritons have a negligible photonic component, of order  $v_{\text{EIT}}/c$ , guaranteeing the excitation of a Rydberg atom per each propagating photon at any given time. The strong dipolar forces between two Rydberg atoms thus effectively mediate interaction between the two propagating photons.

#### A. Two-photon dynamics

Gorshkov *et al.* (2011) provided a quantum description for two photons, which we now follow. A probe photon in the form of a polariton blocks EIT for the second probe photon, which experiences the response

$$t_k^{N_B} = \exp\left(-\frac{\text{OD}_B}{2} \frac{i\gamma}{\Delta + i\gamma}\right)$$

of bare two-level atoms. The nature of the photon-photon interaction is thus controlled by the detuning of the probe  $\Delta$  from the intermediate atomic state. On-resonance excitation ( $\Delta = 0$ ) leads to scattering of the second photon, inducing an effective *dissipative* interaction between the photons. The second photon is scattered inside the blockade sphere with a probability  $1 - e^{-\text{OD}_B}$ . In contrast, for off-resonance excitation ( $|\Delta| \gg \gamma$ ), the second photon experiences much less scattering but acquires a nonzero phase  $\phi = -(\gamma/\Delta)\text{OD}_B/2$ . This leads to a conditional phase shift  $\phi$  for two or more photons, inducing a *dispersive* interaction between the photons. We see that for both on and off resonant processes  $\text{OD}_B$  is the key parameter determining the strength of the effective interaction.

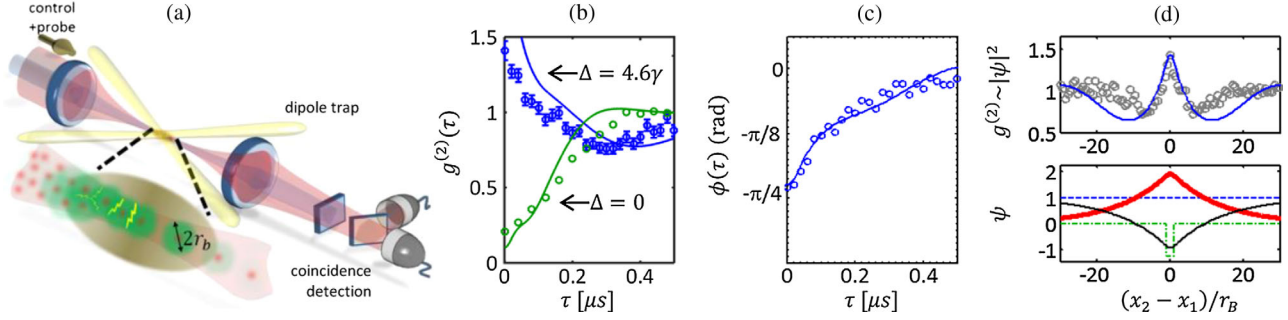


FIG. 15. (a) Schematics of a typical Rydberg-polariton setup: a cloud of ultracold alkali atoms is held between two confocal lenses. The outgoing probe photons are measured using single-photon detectors. (b) Normalized second-order correlation  $g^{(2)}$  of the outgoing probe vs the time separation  $\tau$  between the photons, showing the transition from antibunching in the dissipative regime ( $\Delta = 0$ ) to bunching in the dispersive regime ( $\Delta = 4.6\gamma$ ). The group delay in the medium was  $0.25 \mu\text{s}$ . Points are experimental data, lines are numerical simulations. (c) Conditional phase shift obtained from a tomographic reconstruction of the outgoing two-photon wave function. (d) Signature of the two-photon bound state: The interaction potential  $U(r)$  is approximated by a well of width  $2r_B$  (bottom, dash-dotted line). The resulting bound state, observed in the shape of the measured  $g^{(2)}$  (top, circles, where time is converted to distance via  $x_2 - x_1 = \tau v_{\text{EIT}}$ ), conforms to that calculated using Eq. (43) (top, solid line). The initial state  $\psi(r, 0) = 1$  (bottom, dashed line) is a superposition of the bound state (bottom, thick line) and the manifold of scattering states (bottom, thin line). Adapted from Peyronel *et al.*, 2012, and Firstenberg *et al.*, 2013.

Nonlinear optical response with Rydberg polaritons was demonstrated originally with  $\text{OD}_B \ll 1$  by Pritchard *et al.* (2010). The limit of quantum nonlinearity was afterward reached with  $\text{OD}_B \approx 10$  by Peyronel *et al.* (2012) in a system illustrated in Fig. 15(a). The long axis of an elongated cloud of ultracold atoms was  $L \approx 100 \mu\text{m}$ , and so naively could fit 10 blockade spheres of radius  $r_B \approx 10 \mu\text{m}$ , each containing  $N_B \approx 1000$  atoms. To render an effective 1D system, the light was focused to a diameter larger than the wavelength but smaller than  $r_B$ . In this way, paraxial diffraction did not substantially alter the transverse extent of the photon wave function along its propagation, and, at the same time, two polaritons propagating side by side blocked each other.

Quantum tomography can be used to completely characterize the outgoing two-photon state as a function of the time separation  $\tau$  between the photons (Firstenberg *et al.*, 2013). In particular, it yields the second-order correlation function  $g^{(2)}(\tau)$  and the conditional phase shift  $\phi(\tau)$  relative to the noninteracting case.

The dissipative interaction at  $\Delta = 0$  was observed by Peyronel *et al.* (2012) at an average level of less than one photon in the medium. The probability that two photons exit the medium simultaneously was suppressed by the blockade mechanism, resulting in photon antibunching  $g^{(2)}(0) < 1$ , as seen in Fig. 15(b). The dispersive interaction at  $\Delta \neq 0$  was demonstrated by Firstenberg *et al.* (2013). In addition to a large conditional phase shift  $\phi(0) = 45^\circ$  [Fig. 15(c)], photon bunching  $g^{(2)}(0) > 0$  was observed [Fig. 15(b)].

The bunching in the dispersive regime can be attributed to an effective attractive force between the photons, intuitively arising from an increase in the group velocity inside the blockade volume. To better describe the two-photon dynamics, one defines an effective two-photon wave function inside a medium of length  $L$  as a function of the coordinates  $x_1$  and  $x_2$  of the two photons

$$\psi(x_1, x_2) = \frac{\langle \phi | a(x_1) a(x_2) | \Psi \rangle}{\langle \phi | a(x_1) | \Psi \rangle \langle \phi | a(x_2) | \Psi \rangle}. \quad (42)$$

Here  $|\Psi\rangle$  is the full wave function of the system and  $a(x)$  annihilates a photon at position  $x$ . We assume a stationary scenario with a constant incoming coherent state. Because of symmetry, it is useful to work with the relative  $r = x_2 - x_1$  and mean  $R = (x_1 + x_2)/2$  coordinates. From the definition (42), classical light in the absence of photon-photon interactions is described by  $\psi(r, R) = 1$ ; complete photon blockade corresponds to  $\psi(0, L) = 0$ , which is measured in experiments using  $|\psi(0, L)|^2 = g^{(2)}(0)$ ; and a pure conditional phase  $\phi$  corresponds to  $\psi(0, L) = e^{i\phi}$ .

Firstenberg *et al.* (2013) showed for  $\Omega_c \ll \Delta$  that  $\psi(r, R)$  approximately follows a Schrödinger-like equation with  $R$  playing the role of time,

$$i \frac{\partial \psi}{\partial R} = \frac{4l_a \Delta}{\gamma} \frac{\partial^2 \psi}{\partial r^2} + \frac{\gamma}{l_a \Delta} U(r) \psi. \quad (43)$$

Here  $l_a = L/\text{OD} = 2r_B/\text{OD}_B$  is the attenuation length. Assuming a repulsive van der Waals interaction, the effective potential can be approximated by the step function  $U(|r| \leq r_B) = 1$ . The effective photon mass of this Schrödinger-like evolution originates from the quadratic component ( $\propto k^2$ ) of the dispersion of individual polaritons. This component causes the change in group velocity when the Rydberg level shifts.

Equation (43) approximately describes a potential well. Both the mass and the potential terms flip signs for  $\Delta \rightarrow -\Delta$ , so the effective force remains attractive. The two-photon bound state of the finite-well potential, shown in Fig. 15(d), governs the evolution of an incoming wave function  $\psi(r, 0) = 1$ . In Fig. 15(d), in order to compare the measured  $g^{(2)}(\tau)$  to the calculated  $\psi(r, L)$ , the time  $\tau$  has been converted to distance  $r$  using the group velocity  $v_{\text{EIT}} = l_a \Omega_c^2 / (2\gamma)$ . In experiments,

$\Omega_c^2 \ll c\gamma/l_a$  and thus  $v_{\text{EIT}} \ll c$ , as assumed throughout this section.

Following this initial model, [Bienias \*et al.\* \(2014\)](#) used scattering theory to study the 1D scattering properties for two photons for a wide range of the system parameters. By calculating the effective 1D scattering length, they predicted the existence of scattering resonances analogous to Feshbach resonances in cold atoms, where the interaction turns from attractive to repulsive. For the experimental parameter regime described earlier, [Bienias \*et al.\* \(2014\)](#) generalized Eq. (43) to account for nonstationary (but slowly varying) probe input, essentially replacing the term  $\partial/\partial R$  by  $\partial/\partial R + \partial/(v_{\text{EIT}}\partial t)$ .

Lately, two more treatments for the system have been introduced. [Caneva \*et al.\* \(2015\)](#) modeled the atomic ensemble by a chain of 3LEs along a 1D waveguide, generalizing the input-output formalism presented in the previous sections. With this effective description, they recovered the mean ensemble behavior (e.g., the optical depth and  $v_{\text{EIT}}$ ) and provided a recipe for calculating the high-order correlations of the outgoing photons. In parallel, [Moos \*et al.\* \(2015\)](#) wrote down an exact many-body model for the system, including the loss (scattering out of the system) and the paraxial propagation of the probe light, and provided the conditions under which the model is reduced to an effective many-body system of slow-light polaritons in 1D. They verified the model in the two-photon case by comparing it to exact numerical simulations.

## B. Many photons

Recently, two groups demonstrated *storage* of Rydberg polaritons for implementing a single-photon switch or transistor ([Baur \*et al.\*, 2014](#); [Gorniaczyk \*et al.\*, 2014](#); [Tiarks \*et al.\*, 2014](#)). In these experiments, a “gate” Rydberg polariton is first converted into a stationary excitation (a spin wave) of one Rydberg atom by turning off the control field. Subsequent “signal” polaritons, coupled to a different Rydberg state, are blockaded by the stored polariton. The number of signal photons gated by the stored excitation determines the “gain” of the transistor, recently reaching 100 ([Gorniaczyk \*et al.\*, 2016](#)).

So far, the many-body behavior of Rydberg polaritons has been limited to theoretical studies. [Zeuthen \*et al.\* \(2016\)](#) described the many-body evolution in the dissipative regime, where the system can act to transform a classical input to a regular train of single photons. [Bienias \*et al.\* \(2014\)](#) formulated a low-energy many-body Hamiltonian in the dispersive regime based on their derivation of the 1D scattering length. [Otterbach \*et al.\* \(2013\)](#) introduced an approximate Hamiltonian and used Luttinger liquid theory to predict the Wigner crystallization of Rydberg polaritons. To this end, they assumed an initial transient (preparation) phase where co-located polaritons are scattered out of the system, such that the photon-photon interaction is dominated by the tail of the repulsive van der Waals interaction. [Moos \*et al.\* \(2015\)](#) followed up on these arguments to derive their aforementioned effective many-body model and used numerical calculations (with the DMRG method) to compare with the Luttinger liquid result.

## C. Limitations and prospects

In a long medium ( $L > 2r_B$ ), a copropagating pair of interacting photons traverses several blockade radii. The accumulated effect of the interaction can be calculated from Eq. (43) or from its generalization to the dissipative regime. Such calculations take into account the distortion (dispersion and absorption) of the photon wave packet due to the finite bandwidth of the EIT transmission window, manifested in Eq. (43) by the mass term. The results depend on both OD and  $\text{OD}_B$ , with dissipative interaction ( $\Delta = 0$ ) yielding a blockade probability  $1 - \text{OD}^{-1/2}e^{-\text{OD}_B}$  ([Peyronel \*et al.\*, 2012](#)) and dispersive interaction ( $\Delta \gg \gamma$ ) yielding a conditional phase shift  $\phi \propto \sqrt{\text{OD}} \times \text{OD}_B$  ([Firstenberg \*et al.\*, 2013](#)).

Nevertheless, while OD strengthens the overall effect as implied by these expressions, it is now widely accepted that  $\text{OD}_B \gg 1$  alone is the key condition for high fidelity of quantum information operations. Under this condition, the optimized arrangement is a medium completely residing within one blockade volume ( $L \leq 2r_B$ ) and thus  $\text{OD} = \text{OD}_B \gg 1$ . Intuitively in the copropagating case, this arrangement guarantees that the wave packets of both photons are fully contained within the interaction range ( $r_B$ ), so that the fidelity is not reduced by partial entanglement of different parts of the wave packets. In the case of the aforementioned photonic switch, the gating probability of a “signal” polariton by a stored gate polariton equals  $1 - e^{-\text{OD}_B}$  and the decoherence of the gate during the operation scales as  $e^{-\text{OD}_B}$  ([Li and Lesanovsky, 2015](#); [Murray, Gorshkov, and Pohl, 2016](#)); the overall infidelity of the switch is thus governed by the inefficiency of storage and retrieval of the gate, scaling unfavorably as  $1/\text{OD}_B = 1/\text{OD}$  ([Gorshkov \*et al.\*, 2007](#)). For realizing strongly correlated many-body states of copropagating photons, such as the photon train or the Wigner crystal, the requirements on  $\text{OD}_B$  become even more stringent ([Otterbach \*et al.\*, 2013](#); [Zeuthen \*et al.\*, 2016](#)).

So far, experiments have reached  $\text{OD} = \text{OD}_B = 13$  ([Tresp \*et al.\*, 2016](#)). When using a single Rydberg level, [Baur \*et al.\* \(2014\)](#) and [Gaj \*et al.\* \(2014\)](#) predicted a limit  $\text{OD}_B \lesssim 20$  due to the formation of Rydberg molecules at high atomic densities. A particularly promising approach to circumvent this limit is by tuning so-called Förster resonances between two different Rydberg levels ([Tiarks \*et al.\*, 2014](#); [Gorniaczyk \*et al.\*, 2016](#)). Another approach is the introduction of an optical cavity with a finesse  $\mathcal{F}$  around the atomic ensemble, where the condition  $\text{OD}_B \gg 1$  is replaced by  $\mathcal{F}\text{OD}_B \gg 1$  ([Das \*et al.\*, 2016](#)). Such enhancement of the coupling was first demonstrated by [Parigi \*et al.\* \(2012\)](#), and recently long-lived cavity-Rydberg polaritons were realized ([Ningyuan \*et al.\*, 2016](#)).

## V. CONCLUSIONS AND PERSPECTIVES

Advances in both quantum optics and classical nonlinear optics were fueled by developments in laser, material, and electronic technologies, but apart from occasional intersections these two fields remained almost separated for half a century. Research was mostly limited to the study of either high-intensity fields with macroscopic or mesoscopic materials or low-intensity fields with individual atoms. It is the recent development in realizing and understanding effective

strong photon-photon interactions at low light intensities in various systems that triggered the new field of “quantum nonlinear optics” (Chang, Vuletić, and Lukin, 2014).

There has been significant progress in theoretically describing nonlinear, out-of-equilibrium dynamics of scattered photons from individual emitters in a 1D continuum. A large set of all-optical quantum devices and logic, such as single-photon routers and switches, few-photon optical diodes, and conditional phase gates, has been proposed using individual two- or multilevel emitters in 1D. Some of these could find potential applications in future optical quantum circuits. However, our current understanding of light-matter interactions in the mesoscopic regime, with an ensemble of intrinsically interacting or noninteracting emitters, and the ensuing strongly correlated dynamics, is still at its infancy. This mesoscopic quantum regime was addressed earlier in theoretical studies of quantum solitons in optical fibers (Drummond *et al.*, 1993). Hydrodynamic as well as microscopic descriptions were developed to investigate strong light-matter interaction in this regime. However, the intrinsic nonequilibrium nature of the current experimental systems calls for more careful investigation to obtain a fully quantum mechanical theory in the mesoscopic regime. Numerical methods, especially time-dependent DMRG, may play an important role.

The dynamics of strongly confined propagating photons interacting with multiple emitters is similar to the nonequilibrium dynamics of many-body condensed-matter systems, but still shows some important differences. One significant feature of photonic systems is the controllability over their parameters, including the strength of the interactions and dissipation. This makes the photonic systems suitable candidates for performing quantum simulation of condensed-matter phenomena. Nevertheless, it is also of fundamental interest to investigate quantum nonlinear dynamics in the regime where the number of particles (i.e., photons) is not conserved. This is a unique feature of photonic systems compared to natural closed material systems. In particular, it is interesting to explore the role of loss and dissipation in the quantum-to-classical transition of mesoscopic many-body systems. The interplay of spin-orbit interactions and the collective scattering of light has not been studied so far, and it is an important direction for future studies. In the presence of disorder, these nonlinear systems have the potential to exhibit many-body localization of photons, which has been very little explored theoretically or experimentally.

In a few short years, the experimental efforts with scattering of microwave photons from superconducting artificial atoms and with Rydberg polaritons in cold atomic ensembles have produced multiple interesting and important results. So far, the majority of the results with superconducting systems have involved only a single artificial atom. However, these systems are well suited for scaling up to more atoms. The standard nanofabrication techniques employed in making the devices studied here can easily produce devices of many atoms with well-controlled spacing, coupling, detunings, etc. The range of possible experiments is diverse, ranging from exploring fundamental physics of mesoscopic atom-photon systems to more sophisticated devices for quantum nodes. In addition to increasing the system size, superconducting circuits have room to increase the atom-photon coupling strengths into

new regimes that have not been explored experimental in any system. In fact, ultrastrong coupling, where  $\Gamma \sim \omega_e$ , was recently demonstrated experimentally (Peropadre *et al.*, 2013; Sanchez-Burillo *et al.*, 2014; Forn-Díaz *et al.*, 2017). The ultrastrong-coupling regime promises many new surprises.

At the same time, we saw that strong photon-photon interactions are also enabled in the weak-coupling regime by the action of atomic cooperativity in an ensemble. Rydberg atoms, in particular, exhibit such cooperativity via the blockade mechanism. The dipolar interaction between the Rydberg atoms conceptually transforms the blockade sphere to a two-level superatom, replacing the 2LE of the strong-coupling regime. In both regimes, the photon-photon interaction is governed by the two-photon bound states and changes its nature depending on the frequency detuning. However, while a strongly coupled 2LE preserves the photon number in the channel, the resonant response of the superatom is predominantly lossy (while the superatom is transparent due to EIT for a single photon on resonance, it scatters the subsequent photons, which is exactly the opposite of a 2LE). Consequently, the reflection associated with a strongly coupled 2LE is negligible in the superatom case. The large extent of the superatom relatively to the optical wavelength also contributes to the diminishing of reflection.

Some directions are being studied in both the 2LE and the Rydberg systems, such as nonlinear transmission at the few-photon level, switching and photonic transistors, conditional phase gates, production of bunched or antibunched light, and deterministic entanglement of initially independent photons. The distinct features of the Rydberg systems make them suitable to pursue a variety of rich two-body phenomena, such as a finite-size photonic molecule and exotic many-body behavior, particularly photon crystallization. With the increasing understanding of the capabilities and the limitations of the experimental systems, further developments are soon to be implemented in the preparation of the atomic medium, the atomic excitation schemes, and the optical mode confinement. We expect the field to continue evolving alongside the single-emitter systems and predict that many of the existing ideas, and certainly more to come, will be realized in the near future.

## ACKNOWLEDGMENTS

We are grateful to many colleagues for discussion and guidance, including C. S. Adams, H. U. Baranger, N. Bondyopadhyaya, H. P. Büchler, Y.-L. L. Fang, A. V. Gorshkov, S. Hofferberth, G. Johansson, M. D. Lukin, F. Nori, T. Peyronel, T. Pohl, V. Vuletic, and S. Xu. D. R. acknowledges funding from the Department of Science and Technology, India via the Ramanujan Fellowship. C. M. W. acknowledges financial support from NSERC of Canada, Industry Canada, and the Government of Ontario. O. F. acknowledges support by the Israel Science Foundation and ICORE, the European Research Council starting investigator grant Q-PHOTONICS 678674, the Minerva Foundation, the Sir Charles Clore research prize, and the Laboratory in Memory of Leon and Blacky Broder.

## APPENDIX: DERIVATION OF THE INPUT-OUTPUT FORMALISM

The effective Hamiltonian of a two-level emitter coupled to a chiral (right-moving) photon mode in 1D continuum is given by

$$H_{io}^c/\hbar = \int_{-\infty}^{\infty} dk v_g k a_{R,k}^\dagger a_{R,k} + \frac{1}{2} \omega_e \sigma_z + \frac{V}{\sqrt{2\pi}} \int_{-\infty}^{\infty} dk [a_{R,k}^\dagger \sigma_- + \sigma_+ a_{R,k}]. \quad (\text{A1})$$

The Heisenberg equations of motion for the operators are

$$\frac{da_{R,k}}{dt} = -i v_g k a_{R,k} - \frac{iV}{\sqrt{2\pi}} \sigma_-, \quad (\text{A2})$$

$$\frac{d\sigma_-}{dt} = -i \omega_e \sigma_- + \frac{iV}{\sqrt{2\pi}} \int dk \sigma_z a_{R,k}, \quad (\text{A3})$$

$$\frac{d\sigma_z}{dt} = \frac{2iV}{\sqrt{2\pi}} \int dk (a_{R,k}^\dagger \sigma_- - \sigma_+ a_{R,k}). \quad (\text{A4})$$

Equation (A2) is formally solved by multiplying it by  $e^{iv_g kt}$  and integrating from an initial time  $t_0 < t$  to get

$$a_{R,k}(t) = a_{R,k}(t_0) e^{-iv_g k(t-t_0)} - \frac{iV}{\sqrt{2\pi}} \int_{t_0}^t dt' \sigma_-(t') e^{iv_g k(t'-t)}. \quad (\text{A5})$$

Next we integrate Eq. (A5) with respect to  $k$  and introduce a field operator

$$\Phi(t) = b_{R,\text{in}}(t) - i \frac{V}{2v_g} \sigma_-(t), \quad (\text{A6})$$

where  $\Phi(t) = (1/\sqrt{2\pi}) \int dk a_{R,k}(t)$ , and an input operator (Fan, Kocabaş, and Shen, 2010)

$$b_{R,\text{in}}(t) = \frac{1}{\sqrt{2\pi}} \int dk a_{R,k}(t_0) e^{-iv_g k(t-t_0)}. \quad (\text{A7})$$

Plugging Eq. (A6) into Eqs. (A3) and (A4), we get

$$\frac{d\sigma_-}{dt} = iV \sigma_z b_{R,\text{in}}(t) - \frac{\Gamma}{2} \sigma_- - i \omega_e \sigma_-, \quad (\text{A8})$$

$$\frac{dN_e}{dt} = -iV [\sigma_+ b_{R,\text{in}}(t) - b_{R,\text{in}}^\dagger(t) \sigma_-] - \Gamma N_e, \quad (\text{A9})$$

where  $\Gamma = V^2/v_g$  and  $N_e = (\sigma_z + 1)/2$ . Similarly by integrating Eq. (A2) up to a final time  $t_1 > t$ , we find

$$\Phi(t) = b_{R,\text{out}}(t) + i \frac{V}{2v_g} \sigma_-(t). \quad (\text{A10})$$

Finally we can write from Eqs. (A6) and (A10)

$$b_{R,\text{out}}(t) = b_{R,\text{in}}(t) - i \frac{V}{v_g} \sigma_-(t). \quad (\text{A11})$$

## REFERENCES

- Abdumalikov, A. A., O. Astafiev, A. M. Zagoskin, Y. A. Pashkin, Y. Nakamura, and J. S. Tsai, 2010, *Phys. Rev. Lett.* **104**, 193601.
- Afzelius, M., N. Sangouard, G. Johansson, M. Staudt, and C. Wilson, 2013, *New J. Phys.* **15**, 065008.
- Agarwal, G. S., 2013, *Quantum optics* (Cambridge University Press, Cambridge, 2013).
- Akimov, A. V., A. Mukherjee, C. L. Yu, D. E. Chang, A. S. Zibrov, P. R. Hemmer, H. Park, and M. D. Lukin, 2007, *Nature (London)* **450**, 402.
- Akselrod, G. M., C. Argyropoulos, T. B. Hoang, C. Ciracì, C. Fang, J. Huang, D. R. Smith, and M. H. Mikkelsen, 2014, *Nat. Photonics* **8**, 835.
- Amsüss, R., *et al.*, 2011, *Phys. Rev. Lett.* **107**, 060502.
- Andrews, R., R. Peterson, T. Purdy, K. Cicak, R. Simmonds, C. Regal, and K. Lehnert, 2014, *Nat. Phys.* **10**, 321.
- Angelakis, D. G., M. Huo, E. Kyoseva, and L. C. Kwek, 2011, *Phys. Rev. Lett.* **106**, 153601.
- Anisimov, P. M., J. P. Dowling, and B. C. Sanders, 2011, *Phys. Rev. Lett.* **107**, 163604.
- Aoki, T., A. S. Parkins, D. J. Alton, C. A. Regal, B. Dayan, E. Ostby, K. J. Vahala, and H. J. Kimble, 2009, *Phys. Rev. Lett.* **102**, 083601.
- Arcari, M., *et al.*, 2014, *Phys. Rev. Lett.* **113**, 093603.
- Astafiev, O., A. M. Zagoskin, A. Abdumalikov, Y. A. Pashkin, T. Yamamoto, K. Inomata, Y. Nakamura, and J. Tsai, 2010, *Science* **327**, 840.
- Astafiev, O. V., A. A. Abdumalikov, A. M. Zagoskin, Y. A. Pashkin, Y. Nakamura, and J. S. Tsai, 2010, *Phys. Rev. Lett.* **104**, 183603.
- Babinec, T. M., B. J. Hausmann, M. Khan, Y. Zhang, J. R. Maze, P. R. Hemmer, and M. Lončar, 2010, *Nat. Nanotechnol.* **5**, 195.
- Badolato, A., K. Hennessy, M. Atatüre, J. Dreiser, E. Hu, P. M. Petroff, and A. Imamoglu, 2005, *Science* **308**, 1158.
- Bajcsy, M., S. Hofferberth, V. Balic, T. Peyronel, M. Hafezi, A. S. Zibrov, V. Vuletic, and M. D. Lukin, 2009, *Phys. Rev. Lett.* **102**, 203902.
- Baur, S., D. Tiarks, G. Rempe, and S. Dürr, 2014, *Phys. Rev. Lett.* **112**, 073901.
- Bienias, P., S. Choi, O. Firstenberg, M. F. Maghrebi, M. Gullans, M. D. Lukin, A. V. Gorshkov, and H. P. Büchler, 2014, *Phys. Rev. A* **90**, 053804.
- Birnbaum, K. M., A. Boca, R. Miller, A. D. Boozer, T. E. Northup, and H. J. Kimble, 2005, *Nature (London)* **436**, 87.
- Blais, A., R.-S. Huang, A. Wallraff, S. Girvin, and R. J. Schoelkopf, 2004, *Phys. Rev. A* **69**, 062320.
- Bliokh, K. Y., D. Smirnova, and F. Nori, 2015, *Science* **348**, 1448.
- Bochmann, J., A. Vainsencher, D. D. Awschalom, and A. N. Cleland, 2013, *Nat. Phys.* **9**, 712.
- Boller, K.-J., A. Imamoglu, and S. E. Harris, 1991, *Phys. Rev. Lett.* **66**, 2593.
- Bushev, P., A. K. Feofanov, H. Rotzinger, I. Protodopov, J. H. Cole, C. M. Wilson, G. Fischer, A. Lukashenko, and A. V. Ustinov, 2011, *Phys. Rev. B* **84**, 060501.
- Caldeira, A., and A. J. Leggett, 1983, *Ann. Phys. (N.Y.)* **149**, 374.
- Caneva, T., M. T. Manzoni, T. Shi, J. S. Douglas, J. I. Cirac, and D. E. Chang, 2015, *New J. Phys.* **17**, 113001.
- Carter, S. G., T. M. Sweeney, M. Kim, C. S. Kim, D. Solenov, S. E. Economou, T. L. Reinecke, L. Yang, A. S. Bracker, and D. Gammon, 2013, *Nat. Photonics* **7**, 329.
- Carusotto, I., and C. Ciuti, 2013, *Rev. Mod. Phys.* **85**, 299.
- Chang, D., V. Gritsev, G. Morigi, V. Vuletić, M. Lukin, and E. Demler, 2008, *Nat. Phys.* **4**, 884.

- Chang, D. E., L. Jiang, A. V. Gorshkov, and H. J. Kimble, 2012, *New J. Phys.* **14**, 063003.
- Chang, D. E., A. S. Sørensen, E. A. Demler, and M. D. Lukin, 2007, *Nat. Phys.* **3**, 807.
- Chang, D. E., V. Vuletić, and M. D. Lukin, 2014, *Nat. Photonics* **8**, 685.
- Chen, Y., T. R. Nielsen, N. Gregersen, P. Lodahl, and J. Mørk, 2010, *Phys. Rev. B* **81**, 125431.
- Cheng, Z., and G. Kurizki, 1995, *Phys. Rev. Lett.* **75**, 3430.
- Chiorescu, I., P. Bertet, K. Semba, Y. Nakamura, C. J. P. M. Harmans, and J. E. Mooij, 2004, *Nature (London)* **431**, 159.
- Ciccarello, F., D. E. Browne, L. C. Kwek, H. Schomerus, M. Zarccone, and S. Bose, 2012, *Phys. Rev. A* **85**, 050305.
- Claudon, J., J. Bleuse, N. S. Malik, M. Bazin, P. Jaffrennou, N. Gregersen, C. Sauvan, P. Lalanne, and J.-M. Gérard, 2010, *Nat. Photonics* **4**, 174.
- Costi, T., and G. Zarand, 1999, *Phys. Rev. B* **59**, 12398.
- Cronenwett, S. M., T. H. Oosterkamp, and L. P. Kouwenhoven, 1998, *Science* **281**, 540.
- Das, S., A. Grankin, I. Iakoupov, E. Brion, J. Borregaard, R. Boddeda, I. Usmani, A. Ourjoumtsev, P. Grangier, and A. S. Sørensen, 2016, *Phys. Rev. A* **93**, 040303.
- Dayan, B., A. S. Parkins, T. Aoki, E. P. Ostby, K. J. Vahala, and H. J. Kimble, 2008, *Science* **319**, 1062.
- De Greve, K., *et al.*, 2012, *Nature (London)* **491**, 421.
- Deleglise, S., I. Dotsenko, C. Sayrin, J. Bernu, M. Brune, J.-M. Raimond, and S. Haroche, 2008, *Nature (London)* **455**, 510.
- Deutsch, I. H., R. Y. Chiao, and J. C. Garrison, 1992, *Phys. Rev. Lett.* **69**, 3627.
- DeVoe, R. G., and R. G. Brewer, 1996, *Phys. Rev. Lett.* **76**, 2049.
- Dhar, A., D. Sen, and D. Roy, 2008, *Phys. Rev. Lett.* **101**, 066805.
- DiCarlo, L., *et al.*, 2009, *Nature (London)* **460**, 240.
- Drummond, P., R. Shelby, S. Friberg, and Y. Yamamoto, 1993, *Nature (London)* **365**, 307.
- Dzsotjan, D., A. S. Sørensen, and M. Fleischhauer, 2010, *Phys. Rev. B* **82**, 075427.
- Englund, D., A. Faraon, I. Fushman, N. Stoltz, P. Petroff, and J. Vučković, 2007, *Nature (London)* **450**, 857.
- Eschner, J., C. Raab, F. Schmidt-Kaler, and R. Blatt, 2001, *Nature (London)* **413**, 495.
- Faez, S., P. Türschmann, H. R. Haakh, S. Götzinger, and V. Sandoghdar, 2014, *Phys. Rev. Lett.* **113**, 213601.
- Fan, B., G. Johansson, J. Combes, G. J. Milburn, and T. M. Stace, 2014, *Phys. Rev. B* **90**, 035132.
- Fan, B., A. F. Kockum, J. Combes, G. Johansson, I.-c. Hoi, C. M. Wilson, P. Delsing, G. J. Milburn, and T. M. Stace, 2013, *Phys. Rev. Lett.* **110**, 053601.
- Fan, S., Ş. E. Kocabaş, and J.-T. Shen, 2010, *Phys. Rev. A* **82**, 063821.
- Fang, Y.-L. L., and H. U. Baranger, 2015, *Phys. Rev. A* **91**, 053845.
- Fang, Y.-L. L., H. Zheng, and H. U. Baranger, 2014, *EPJ Quantum Techno.* **1**, 3.
- Faraon, A., E. Waks, D. Englund, I. Fushman, and J. Vučković, 2007, *Appl. Phys. Lett.* **90**, 073102.
- Firstenberg, O., T. Peyronel, Q.-Y. Liang, A. V. Gorshkov, M. D. Lukin, and V. Vuletić, 2013, *Nature (London)* **502**, 71.
- Fleischhauer, M., A. Imamoglu, and J. P. Marangos, 2005, *Rev. Mod. Phys.* **77**, 633.
- Fleischhauer, M., and M. D. Lukin, 2000, *Phys. Rev. Lett.* **84**, 5094.
- Forn-Díaz, P., J. J. García-Ripoll, B. Peropadre, M. A. Yurtalan, J.-L. Orgiazzi, R. Belyansky, C. M. Wilson, and A. Lupascu, 2017, *Nat. Phys.* **13**, 39.
- Frattini, F., E. Mascarenhas, L. Safari, J.-P. Poizat, D. Valente, A. Auffèves, D. Gerace, and M. F. Santos, 2014, *Phys. Rev. Lett.* **113**, 243601.
- Friedler, I., D. Petrosyan, M. Fleischhauer, and G. Kurizki, 2005, *Phys. Rev. A* **72**, 043803.
- Fushman, I., D. Englund, A. Faraon, N. Stoltz, P. Petroff, and J. Vučković, 2008, *Science* **320**, 769.
- Gaj, A., A. T. Krupp, J. B. Balewski, R. Löw, S. Hofferberth, and T. Pfau, 2014, *Nat. Commun.* **5**, 4546.
- Gao, W., P. Fallahi, E. Togan, J. Miguel-Sánchez, and A. Imamoglu, 2012, *Nature (London)* **491**, 426.
- Gardiner, C. W., and M. J. Collett, 1985, *Phys. Rev. A* **31**, 3761.
- Gerace, D., H. E. Türeci, A. Imamoglu, V. Giovannetti, and R. Fazio, 2009, *Nat. Phys.* **5**, 281.
- Gibbs, H. M., 1985, *Optical Bistability: Controlling Light with Light* (Academic, Orlando, FL).
- Girvin, S. M., M. H. Devoret, and R. J. Schoelkopf, 2009, *Phys. Scr.* **T137**, 014012.
- Goban, A., *et al.*, 2014, *Nat. Commun.* **5**, 3808.
- Goldhaber-Gordon, D., H. Shtrikman, D. Mahalu, D. Abusch-Magder, U. Meirav, and M. Kastner, 1998, *Nature (London)* **391**, 156.
- Goldstein, E. V., and P. Meystre, 1997, *Phys. Rev. A* **56**, 5135.
- Gonzalez-Tudela, A., D. Martin-Cano, E. Moreno, L. Martin-Moreno, C. Tejedor, and F. J. Garcia-Vidal, 2011, *Phys. Rev. Lett.* **106**, 020501.
- Gorniaczyk, H., C. Tresp, P. Bienias, A. Paris-Mandoki, W. Li, I. Mirgorodskiy, H. Büchler, I. Lesanovsky, and S. Hofferberth, 2016, *Nat. Commun.* **7**, 12480.
- Gorniaczyk, H., C. Tresp, J. Schmidt, H. Fedder, and S. Hofferberth, 2014, *Phys. Rev. Lett.* **113**, 053601.
- Gorshkov, A. V., A. André, M. D. Lukin, and A. S. Sørensen, 2007, *Phys. Rev. A* **76**, 033805.
- Gorshkov, A. V., J. Otterbach, M. Fleischhauer, T. Pohl, and M. D. Lukin, 2011, *Phys. Rev. Lett.* **107**, 133602.
- Greenberg, Y. S., and A. A. Shtygashev, 2015, *Phys. Rev. A* **92**, 063835.
- Greentree, A. D., C. Tahan, J. H. Cole, and L. C. Hollenberg, 2006, *Nat. Phys.* **2**, 856.
- Grezes, C., *et al.*, 2014, *Phys. Rev. X* **4**, 021049.
- Guerlin, C., J. Bernu, S. Deleglise, C. Sayrin, S. Gleyzes, S. Kuhr, M. Brune, J.-M. Raimond, and S. Haroche, 2007, *Nature (London)* **448**, 889.
- Haroche, S., and J.-M. Raimond, 2013, *Exploring the Quantum: Atoms, Cavities, and Photons* (Oxford University Press, New York).
- Harris, S. E., J. E. Field, and A. Imamoglu, 1990, *Phys. Rev. Lett.* **64**, 1107.
- Hartmann, M. J., F. G. Brandao, and M. B. Plenio, 2006, *Nat. Phys.* **2**, 849.
- Hennessy, K., A. Badolato, M. Winger, D. Gerace, M. Atatüre, S. Gulde, S. Fält, E. L. Hu, and A. Imamoglu, 2007, *Nature (London)* **445**, 896.
- Hensen, B., *et al.*, 2015, *Nature (London)* **526**, 682.
- Hoi, I.-C., A. F. Kockum, T. Palomaki, T. M. Stace, B. Fan, L. Tornberg, S. R. Sathyamoorthy, G. Johansson, P. Delsing, and C. M. Wilson, 2013, *Phys. Rev. Lett.* **111**, 053601.
- Hoi, I.-C., A. F. Kockum, L. Tornberg, A. Pourkabirian, G. Johansson, P. Delsing, and C. M. Wilson, 2015, *Nat. Phys.* **11**, 1045.
- Hoi, I.-C., T. Palomaki, J. Lindkvist, G. Johansson, P. Delsing, and C. Wilson, 2012, *Phys. Rev. Lett.* **108**, 263601.
- Hoi, I.-C., C. Wilson, G. Johansson, J. Lindkvist, B. Peropadre, T. Palomaki, and P. Delsing, 2013, *New J. Phys.* **15**, 025011.

- Hoi, I.-C., C. M. Wilson, G. Johansson, T. Palomaki, B. Peropadre, and P. Delsing, 2011, *Phys. Rev. Lett.* **107**, 073601.
- Iacopini, E., and E. Zavattini, 1979, *Phys. Lett. B* **85**, 151.
- Imamoğlu, A., H. Schmidt, G. Woods, and M. Deutsch, 1997, *Phys. Rev. Lett.* **79**, 1467.
- Inomata, K., K. Koshino, Z. R. Lin, W. D. Oliver, J. S. Tsai, Y. Nakamura, and T. Yamamoto, 2014, *Phys. Rev. Lett.* **113**, 063604.
- Jalas, D., *et al.*, 2013, *Nat. Photonics* **7**, 579.
- Javadi, A., *et al.*, 2015, *Nat. Commun.* **6**, 8655.
- Julsgaard, B., C. Grezes, P. Bertet, and K. Mølmer, 2013, *Phys. Rev. Lett.* **110**, 250503.
- Karplus, R., and M. Neuman, 1951, *Phys. Rev.* **83**, 776.
- Kimble, H. J., 2008, *Nature (London)* **453**, 1023.
- Kimble, H. J., M. Dagenais, and L. Mandel, 1977, *Phys. Rev. Lett.* **39**, 691.
- Korz, B., C. C. W. Lim, R. Houlmann, N. Gisin, M. J. Li, D. Nolan, B. Sanguinetti, R. Thew, and H. Zbinden, 2015, *Nat. Photonics* **9**, 163.
- Koshino, K., S. Ishizaka, and Y. Nakamura, 2010, *Phys. Rev. A* **82**, 010301.
- Koshino, K., and Y. Nakamura, 2012, *New J. Phys.* **14**, 043005.
- Kubo, Y., *et al.*, 2011, *Phys. Rev. Lett.* **107**, 220501.
- Kühn, S., U. Håkanson, L. Rogobete, and V. Sandoghdar, 2006, *Phys. Rev. Lett.* **97**, 017402.
- Laakso, M., and M. Pletyukhov, 2014, *Phys. Rev. Lett.* **113**, 183601.
- Lalumière, K., B. C. Sanders, A. F. van Loo, A. Fedorov, A. Wallraff, and A. Blais, 2013, *Phys. Rev. A* **88**, 043806.
- Laucht, A., *et al.*, 2012, *Phys. Rev. X* **2**, 011014.
- Le Feber, B., N. Rotenberg, and L. Kuipers, 2015, *Nat. Commun.* **6**, 6695.
- Leggett, A. J., S. Chakravarty, A. Dorsey, M. P. Fisher, A. Garg, and W. Zwerger, 1987, *Rev. Mod. Phys.* **59**, 1.
- Lehmberg, R. H., 1970, *Phys. Rev. A* **2**, 883.
- Li, T. Y., J. F. Huang, and C. K. Law, 2015, *Phys. Rev. A* **91**, 043834.
- Li, W., and I. Lesanovsky, 2015, *Phys. Rev. A* **92**, 043828.
- Liao, J.-Q., and C. Law, 2010, *Phys. Rev. A* **82**, 053836.
- Lin, Q., J. Rosenberg, D. Chang, R. Camacho, M. Eichenfield, K. J. Vahala, and O. Painter, 2010, *Nat. Photonics* **4**, 236.
- Lodahl, P., S. Mahmoodian, and S. Stobbe, 2015, *Rev. Mod. Phys.* **87**, 347.
- Longo, P., P. Schmitteckert, and K. Busch, 2010, *Phys. Rev. Lett.* **104**, 023602.
- Lukin, M. D., M. Fleischhauer, R. Cote, L. M. Duan, D. Jaksch, J. I. Cirac, and P. Zoller, 2001, *Phys. Rev. Lett.* **87**, 037901.
- Mabuchi, H., and A. C. Doherty, 2002, *Science* **298**, 1372.
- Maser, A., B. Gmeiner, T. Utikal, S. Götzinger, and V. Sandoghdar, 2016, *Nat. Photonics* **10**, 450.
- Matsuda, N., R. Shimizu, Y. Mitsumori, H. Kosaka, and K. Edamatsu, 2009, *Nat. Photonics* **3**, 95.
- Mehta, P., and N. Andrei, 2006, *Phys. Rev. Lett.* **96**, 216802.
- Meir, Y., N. S. Wingreen, and P. A. Lee, 1991, *Phys. Rev. Lett.* **66**, 3048.
- Meir, Z., O. Schwartz, E. Shahmoon, D. Oron, and R. Ozeri, 2014, *Phys. Rev. Lett.* **113**, 193002.
- Milburn, G., 1989, *Phys. Rev. Lett.* **62**, 2124.
- Miller, R., T. E. Northup, K. M. Birnbaum, A. Boca, A. D. Boozer, and H. J. Kimble, 2005, *J. Phys. B* **38**, S551.
- Mitsch, R., C. Sayrin, B. Albrecht, P. Schneeweiss, and A. Rauschenbeutel, 2014, *Nat. Commun.* **5**, 5713.
- Moos, M., M. Höning, R. Unanyan, and M. Fleischhauer, 2015, *Phys. Rev. A* **92**, 053846.
- Müller, M., I. Lesanovsky, H. Weimer, H. P. Büchler, and P. Zoller, 2009, *Phys. Rev. Lett.* **102**, 170502.
- Munro, W., K. Nemoto, R. Beausoleil, and T. Spiller, 2005, *Phys. Rev. A* **71**, 033819.
- Murray, C. R., A. V. Gorshkov, and T. Pohl, 2016, [arXiv:1607.01984](https://arxiv.org/abs/1607.01984).
- Napolitano, M., M. Koschorreck, B. Dubost, N. Behbood, R. J. Sewell, and M. W. Mitchell, 2011, *Nature (London)* **471**, 486.
- Neumeier, L., M. Leib, and M. J. Hartmann, 2013, *Phys. Rev. Lett.* **111**, 063601.
- Newton, R. G., 1982, *Scattering Theory of Waves and Particles* (Springer-Verlag, New York), 2nd ed.
- Ningyuan, J., A. Georgakopoulos, A. Ryou, N. Schine, A. Sommer, and J. Simon, 2016, *Phys. Rev. A* **93**, 041802.
- Nishino, A., T. Imamura, and N. Hatano, 2011, *Phys. Rev. B* **83**, 035306.
- Nogues, G., A. Rauschenbeutel, S. Osnaghi, M. Brune, J. M. Raimond, and S. Haroche, 1999, *Nature (London)* **400**, 239.
- Notomi, M., E. Kuramochi, and T. Tanabe, 2008, *Nat. Photonics* **2**, 741.
- Novikov, S., T. Sweeney, J. Robinson, S. Premaratne, B. Suri, F. Wellstood, and B. Palmer, 2016, *Nat. Phys.* **12**, 75.
- Otterbach, J., M. Moos, D. Muth, and M. Fleischhauer, 2013, *Phys. Rev. Lett.* **111**, 113001.
- Parigi, V., E. Bimbard, J. Stanojevic, A. J. Hilliard, F. Nogrette, R. Tualle-Brouri, A. Ourjoumtsev, and P. Grangier, 2012, *Phys. Rev. Lett.* **109**, 233602.
- Park, H.-G., C. J. Barrelet, Y. Wu, B. Tian, F. Qian, and C. M. Lieber, 2008, *Nat. Photonics* **2**, 622.
- Paul, H., 1982, *Rev. Mod. Phys.* **54**, 1061.
- Peropadre, B., J. Lindkvist, I.-C. Hoi, C. Wilson, J. J. Garcia-Ripoll, P. Delsing, and G. Johansson, 2013, *New J. Phys.* **15**, 035009.
- Perrella, C., P. S. Light, J. D. Anstie, F. Benabid, T. M. Stace, A. G. White, and A. N. Luiten, 2013, *Phys. Rev. A* **88**, 013819.
- Petersen, J., J. Volz, and A. Rauschenbeutel, 2014, *Science* **346**, 67.
- Petrosyan, D., J. Otterbach, and M. Fleischhauer, 2011, *Phys. Rev. Lett.* **107**, 213601.
- Peyronel, T., O. Firstenberg, Q.-Y. Liang, S. Hofferberth, A. V. Gorshkov, T. Pohl, M. D. Lukin, and V. Vuletić, 2012, *Nature (London)* **488**, 57.
- Pritchard, J. D., D. Maxwell, A. Gauguet, K. J. Weatherill, M. P. A. Jones, and C. S. Adams, 2010, *Phys. Rev. Lett.* **105**, 193603.
- Pritchard, J. D., K. J. Weatherill, and C. S. Adams, 2013, *Annu. Rev. Cold At. Mol.* **1**, 301.
- Probst, S., H. Rotzinger, S. Wünsch, P. Jung, M. Jerger, M. Siegel, A. V. Ustinov, and P. A. Bushev, 2013, *Phys. Rev. Lett.* **110**, 157001.
- Putz, S., D. O. Krimer, R. Amsuess, A. Valookaran, T. Noebauer, J. Schmiedmayer, S. Rotter, and J. Majer, 2014, *Nat. Phys.* **10**, 720.
- Raimond, J. M., M. Brune, and S. Haroche, 2001, *Rev. Mod. Phys.* **73**, 565.
- Reinhard, A., T. C. Liebisch, B. Knuffman, and G. Raithel, 2007, *Phys. Rev. A* **75**, 032712.
- Reithmaier, G., M. Kaniber, F. Flassig, S. Lichtmannecker, K. Müller, A. Andrejew, J. Vuckovic, R. Gross, and J. J. Finley, 2015, *Nano Lett.* **15**, 5208.
- Rephaeli, E., and S. Fan, 2012, *Phys. Rev. Lett.* **108**, 143602.
- Rephaeli, E., and S. Fan, 2013, *Photon. Res.* **1**, 110.
- Rephaeli, E., Ş. E. Kocabaş, and S. Fan, 2011, *Phys. Rev. A* **84**, 063832.
- Rephaeli, E., J.-T. Shen, and S. Fan, 2010, *Phys. Rev. A* **82**, 033804.
- Rezus, Y. L. A., S. G. Walt, R. Lettow, A. Renn, G. Zumofen, S. Götzinger, and V. Sandoghdar, 2012, *Phys. Rev. Lett.* **108**, 093601.
- Ritter, S., C. Nölleke, C. Hahn, A. Reiserer, A. Neuzner, M. Uphoff, M. Mücke, E. Figueroa, J. Bochmann, and G. Rempe, 2012, *Nature (London)* **484**, 195.
- Rosenblum, S., A. Borne, and B. Dayan, 2015, [arXiv:1412.0604](https://arxiv.org/abs/1412.0604).

- Roy, D., 2010a, *Phys. Rev. B* **81**, 155117.
- Roy, D., 2010b, *Phys. Rev. B* **81**, 085330.
- Roy, D., 2011a, *Phys. Rev. A* **83**, 043823.
- Roy, D., 2011b, *Phys. Rev. Lett.* **106**, 053601.
- Roy, D., 2013a, *Sci. Rep.* **3**, 2337.
- Roy, D., 2013b, *Phys. Rev. A* **87**, 063819.
- Roy, D., and N. Bondyopadhyaya, 2014, *Phys. Rev. A* **89**, 043806.
- Rupasov, V. I., and V. I. Yudson, 1984a, *Zh. Eksp. Teor. Fiz.* **87**, 1617 [[http://jetp.ac.ru/cgi-bin/dn/e\\_060\\_05\\_0927.pdf](http://jetp.ac.ru/cgi-bin/dn/e_060_05_0927.pdf)].
- Rupasov, V. I., and V. I. Yudson, 1984b, *Zh. Eksp. Teor. Fiz.* **86**, 819 [[http://jetp.ac.ru/cgi-bin/dn/e\\_059\\_03\\_0478.pdf](http://jetp.ac.ru/cgi-bin/dn/e_059_03_0478.pdf)].
- Saffman, M., T. G. Walker, and K. Mølmer, 2010, *Rev. Mod. Phys.* **82**, 2313.
- Sanchez-Burillo, E., D. Zueco, J. J. Garcia-Ripoll, and L. Martin-Moreno, 2014, *Phys. Rev. Lett.* **113**, 263604.
- Sathyamoorthy, S. R., L. Tornberg, A. F. Kockum, B. Q. Baragiola, J. Combes, C. M. Wilson, T. M. Stace, and G. Johansson, 2014, *Phys. Rev. Lett.* **112**, 093601.
- Schuster, I., A. Kubanek, A. Fuhrmanek, T. Puppe, P. W. H. Pinkse, K. Murr, and G. Rempe, 2008, *Nat. Phys.* **4**, 382.
- Schwinger, J., 1951, *Phys. Rev.* **82**, 664.
- Sevinçli, S., N. Henkel, C. Ates, and T. Pohl, 2011, *Phys. Rev. Lett.* **107**, 153001.
- Shen, J.-T., and S. Fan, 2005a, *Opt. Lett.* **30**, 2001.
- Shen, J.-T., and S. Fan, 2005b, *Phys. Rev. Lett.* **95**, 213001.
- Shen, J.-T., and S. Fan, 2007a, *Phys. Rev. A* **76**, 062709.
- Shen, J.-T., and S. Fan, 2007b, *Phys. Rev. Lett.* **98**, 153003.
- Shen, J.-T., and S. Fan, 2009, *Phys. Rev. A* **79**, 023837.
- Shen, Y.-R., 1984, *Principles of nonlinear optics* (Wiley-Interscience, New York).
- Sherson, J. F., H. Krauter, R. K. Olsson, B. Julsgaard, K. Hammerer, I. Cirac, and E. S. Polzik, 2006, *Nature (London)* **443**, 557.
- Shi, T., and C. P. Sun, 2009, *Phys. Rev. B* **79**, 205111.
- Shomroni, I., S. Rosenblum, Y. Lovsky, O. Bechler, G. Guendelman, and B. Dayan, 2014, *Science* **345**, 903.
- Smolyaninov, I. I., J. Elliott, A. V. Zayats, and C. C. Davis, 2005, *Phys. Rev. Lett.* **94**, 057401.
- Staudt, M. U., *et al.*, 2012, *J. Phys. B* **45**, 124019.
- Tabuchi, Y., S. Ishino, T. Ishikawa, R. Yamazaki, K. Usami, and Y. Nakamura, 2014, *Phys. Rev. Lett.* **113**, 083603.
- Taylor, J. R., 2006, *Scattering Theory: The Quantum Theory of Nonrelativistic Collisions* (Dover, New York).
- Thompson, R. J., G. Rempe, and H. J. Kimble, 1992, *Phys. Rev. Lett.* **68**, 1132.
- Tiarks, D., S. Baur, K. Schneider, S. Dürr, and G. Rempe, 2014, *Phys. Rev. Lett.* **113**, 053602.
- Tresp, C., C. Zimmer, I. Mirgorodskiy, H. Gorniaczyk, A. Paris-Mandoki, and S. Hofferberth, 2016, *Phys. Rev. Lett.* **117**, 223001.
- Turchette, Q. A., C. Hood, W. Lange, H. Mabuchi, and H. J. Kimble, 1995, *Phys. Rev. Lett.* **75**, 4710.
- Ursin, R., *et al.*, 2007, *Nat. Phys.* **3**, 481.
- van Enk, S. J., and H. J. Kimble, 2001, *Phys. Rev. A* **63**, 023809.
- van Loo, A. F., A. Fedorov, K. Lalumire, B. C. Sanders, A. Blais, and A. Wallraff, 2013, *Science* **342**, 1494.
- Venkataraman, V., K. Saha, and A. L. Gaeta, 2013, *Nat. Photonics* **7**, 138.
- Versteegh, M. A., M. E. Reimer, K. D. Jöns, D. Dalacu, P. J. Poole, A. Gulinatti, A. Giudice, and V. Zwiller, 2014, *Nat. Commun.* **5**, 5298.
- Vetsch, E., D. Reitz, G. Sagué, R. Schmidt, S. T. Dawkins, and A. Rauschenbeutel, 2010, *Phys. Rev. Lett.* **104**, 203603.
- Vuletic, V., 2006, *Nat. Phys.* **2**, 801.
- Wallraff, A., D. I. Schuster, A. Blais, L. Frunzio, R.-S. Huang, J. Majer, S. Kumar, S. M. Girvin, and R. J. Schoelkopf, 2004, *Nature (London)* **431**, 162.
- Walls, D. F., and G. J. Milburn, 2008, *Quantum Optics* (Springer, New York), 2nd ed.
- Walther, H., B. T. H. Varcoe, B.-G. Englert, and T. Becker, 2006, *Rep. Prog. Phys.* **69**, 1325.
- Witthaut, D., and A. S. Sørensen, 2010, *New J. Phys.* **12**, 043052.
- Xu, S., and S. Fan, 2015, *Phys. Rev. A* **91**, 043845.
- Xu, S., E. Rephaeli, and S. Fan, 2013, *Phys. Rev. Lett.* **111**, 223602.
- Yoshie, T., A. Scherer, J. Hendrickson, G. Khitrova, H. Gibbs, G. Rupper, C. Ell, O. Shchekin, and D. Deppe, 2004, *Nature (London)* **432**, 200.
- Yudson, V. I., and P. Reineker, 2008, *Phys. Rev. A* **78**, 052713.
- Zapasskii, V. S., A. Greilich, S. A. Crooker, Y. Li, G. G. Kozlov, D. R. Yakovlev, D. Reuter, A. D. Wieck, and M. Bayer, 2013, *Phys. Rev. Lett.* **110**, 176601.
- Zavattini, G., U. Gastaldi, R. Pengo, G. Ruoso, F. D. Valle, and E. Milotti, 2012, *Int. J. Mod. Phys. A* **27**, 1260017.
- Zeuthen, E., M. J. Gullans, M. F. Maghrebi, and A. V. Gorshkov, 2016, [arXiv:1608.06068](https://arxiv.org/abs/1608.06068).
- Zheng, H., and H. U. Baranger, 2013, *Phys. Rev. Lett.* **110**, 113601.
- Zheng, H., D. J. Gauthier, and H. U. Baranger, 2010, *Phys. Rev. A* **82**, 063816.
- Zheng, H., D. J. Gauthier, and H. U. Baranger, 2012, *Phys. Rev. A* **85**, 043832.
- Zheng, H., D. J. Gauthier, and H. U. Baranger, 2013, *Phys. Rev. Lett.* **111**, 090502.
- Zhou, L., Z. R. Gong, Y.-x. Liu, C. P. Sun, and F. Nori, 2008, *Phys. Rev. Lett.* **101**, 100501.
- Zhou, P., and S. Swain, 1996, *Phys. Rev. Lett.* **77**, 3995.
- Zumofen, G., N. M. Mojarad, V. Sandoghdar, and M. Agio, 2008, *Phys. Rev. Lett.* **101**, 180404.